

Dynamic π -Bonding of Imidazolyl Substituent in a Formally 16-Electron $\text{Cp}^*\text{Ru}(\kappa^2\text{-P},\text{N})^+$ Catalyst Allows Dramatic Rate Increases in (*E*)-Selective Monoisomerization of Alkenes

Erik R. Paulson,[†] Curtis E. Moore,[‡] Arnold L. Rheingold,[‡] David P. Pullman,[†] Ryan W. Sindewald,[†] Andrew L. Cooksy,[†] and Douglas B. Grotjahn^{*,†}

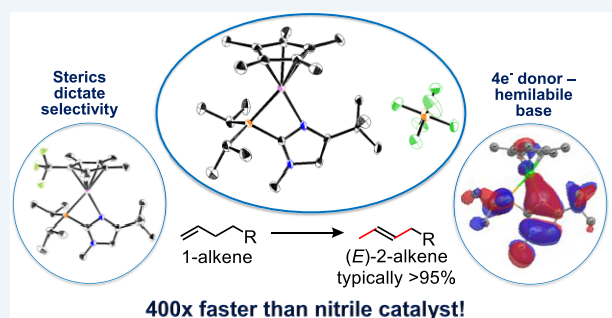
[†]Department of Chemistry and Biochemistry, San Diego State University, 5500 Campanile Drive, San Diego, California 92182-1030, United States

[‡]Department of Chemistry and Biochemistry, University of California, San Diego, 9500 Gilman Drive, La Jolla, California 92093, United States

S Supporting Information

ABSTRACT: Alkene isomerization can be an atom-economical approach to generating a wide range of alkene intermediates for synthesis, but fully equilibrated mixtures of disubstituted internal alkenes typically contain significant amounts of the positional as well as geometric (*E* and *Z*) isomers. Most classical catalyst systems for alkene isomerization struggle to kinetically control either positional or *E/Z* isomerism. We report coordinatively unsaturated, formally 16-electron Cp^*Ru catalyst **5**, which facilitates simultaneous regio- and stereoselective isomerization of linear 1-alkenes to their internal analogues, providing consistent yields of (*E*)-2-alkenes greater than 95%. Because nitrile-free catalyst **5** is more than 400 times faster than previously published nitrile-containing analogues **2** + **2a**, very reasonable 0.1–0.5 mol % loadings of **5** complete ambient-temperature reactions within 15 min to 4 h. UV–vis, NMR, and computational studies depict the imidazolyl fragment on the phosphine as a hemilabile, four-electron donor in $\kappa^2\text{-P},\text{N}$ coordination. For the first time, we show direct experimental evidence that the PN ligand has accepted a proton from the substrate by characterizing the intermediate $\text{Cp}^*\text{Ru}[\eta^3\text{-allyl}][\kappa^1\text{-P}]\text{P}-\text{N}^+\text{H}$, which highlights the essential role of the bifunctional ligand in promoting rapid and selective alkene isomerizations. Moreover, kinetic studies and computations reveal the role of alkene binding in selectivity of unsaturated catalyst **5**.

KEYWORDS: alkenes, isomerization, selectivity, catalyst, bifunctional, π -bonding



INTRODUCTION

While there are a number of catalysts that can achieve selective isomerization for compounds containing specific functional groups such as allylic alcohols,^{1,2} ethers,³ and amines,⁴ few isomerization catalysts exist that can exhibit regio- and/or stereoselectivity in a general fashion for substrates that do not contain branching or other steric factors that could inhibit repeated isomerizations down a chain. There has been a significant improvement in the controlled positional isomerization of 1-alkenes to 2-alkenes in the last 20 years, but most of these catalysts give (*E*)-2 and (*Z*)-2 product in close to thermodynamic ratio of about 4:1 for linear unbranched alkenes.^{5,6}

The challenge is more acute when attempting to control both positional and *E/Z* selectivity. Four recent catalysts that are positional- and (*Z*)-selective are shown in Chart 1 with performances summarized in Table 1. High (*Z*)-selectivity combined with positional selectivity remains an unmet challenge; (*E*)/(*Z*)-ratios for 2-alkenes were in the range 1:5.6 to 1:2.6. The catalyst of Holland et al. acted on linear

alkene substrates but showed signs of deactivation with certain substrates (silyl, dienes) and would not tolerate protic or C=O functionality.⁷ Hilt et al. had significant success with four-component catalyst systems.⁸ For Hilt's Ni system, optimum selectivity required cryogenic temperatures, whereas the Co system operated at room temperature. Dobreiner's system tolerates protic and C=O, silyl, and diene functional groups, although their presence or longer-chain alkenes needed longer reaction times and/or higher catalyst loadings.⁹

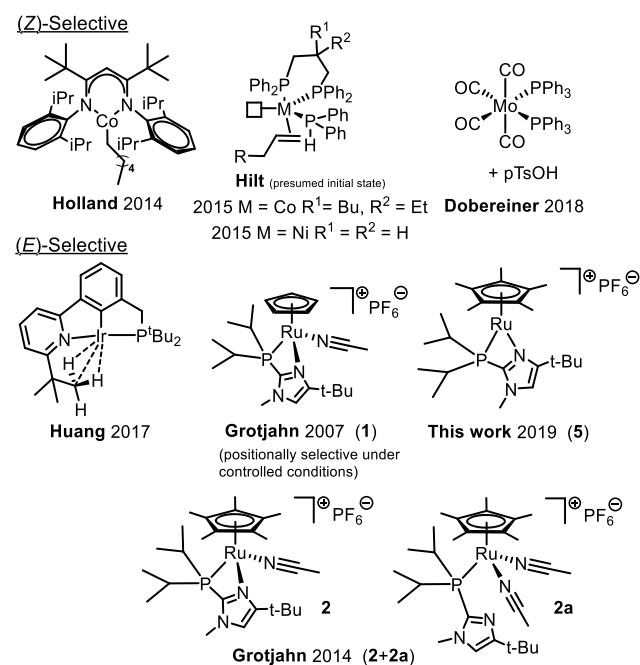
At present, two recent catalysts achieve high positional and (*E*)-selectivities with geometric selectivities higher than those for (*Z*)-selective systems. In 2014, we disclosed the Cp^* analogue of the zipper catalyst **1**¹⁰ (**2** + **2a**, Chart 1) as a mixture of two complexes in equilibrium which can selectively achieve >95% yields of (*E*)-2-alkenes with no detectable (*Z*)-isomers by ¹H NMR and GC and little (<3%) over-

Received: November 5, 2018

Revised: June 21, 2019

Published: July 12, 2019

Chart 1. Geometric and Positionally Selective Alkene Isomerization Catalysts

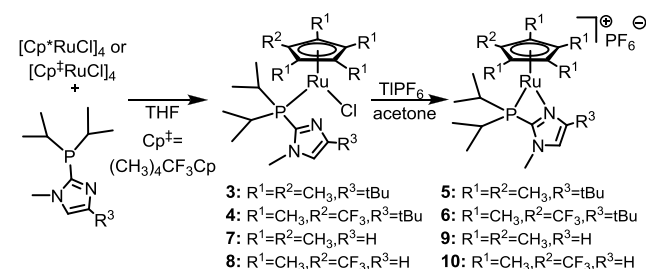


isomerization, all with reasonably low loadings and mild conditions (1 mol %, 40 °C, 48 h). After we started the work reported here, in 2017, Huang et al. reported an iridium pincer complex that generally furnishes 90–95% (*E*)-2 alkenes with 20–50:1 *E/Z* selectivity, also with low loadings and temperatures, though we note the authors purified alkene substrates by distillation from LiAlH₄.¹¹ The suggested mechanism includes oxidative addition of one of the C–H bonds of the pyridine arm of the pincer ligand to generate the hydride for insertion in an alkyl mechanism.¹²

We conclusively showed that the imidazolyl nitrogen in **2a** creates a catalyst that is >3000 times faster than an analogue of **2a** with a P(*i*Pr)₃ ligand.¹³ However, comparing **1** and **2 + 2a**, the price of high positional control by the latter is about 1000-fold reduced in rate. In the search for a more active catalyst, we

considered nitrile-free complex **5** (Scheme 1). Nitrile inhibition had been demonstrated by us on two occasions:

Scheme 1. Synthesis of Complexes 3–10



(1) addition of an equivalent of CH₃CN to **2 + 2a** slowed the catalyst by a factor of 2, and (2) addition of 1.5–2 equiv of CH₃CN slows Cp catalyst **1** but not in a way that prevents isomerization of 2-alkene to 3-alkene.¹³ Hence, our hypothesis was that **5** would be faster than **2 + 2a** because of a lack of competition of nitrile and alkene. As described herein, the synthesis of **5** avoids production of the mixture of **2 + 2a** from which it had proved impossible to remove enough nitrile to make pure mononitrile species **2**. More significantly, here, we show that **5** is more than 400 times faster than **2 + 2a** and about 1/10 as fast as Cp analogue **1**. However, like the **2 + 2a** mixture, **5** has the ability to form (*E*)-2 alkenes in ca. 95% yields and excellent selectivity. Here, we also describe the unusual ability of the ruthenium-bound imidazole ring to engage in π -bonding, thus stabilizing the formally 16-electron Ru center of **5**. Moreover, we show that it is the steric bulk of the Cp* ligand and not its greater electron donation that is responsible for slowing the further positional isomerization. We also show direct evidence for reversible and highly positionally specific binding of alkenes as well as the first direct spectroscopic evidence of the pendent imidazole involved in proton transfer through an allyl intermediate.

RESULTS AND DISCUSSION

Synthesis and Characterization of Complexes. Complex **3** appeared to be an ideal intermediate to make **5** (Scheme

Table 1. Summary of Isomerization of Terminal Linear Alkenes with Selected Catalysts in Chart 1

catalyst	mol % ^a	time (min)	temp (°C)	conv (%)	% 2-alkene	<i>E/Z</i> ratio	TOF (min ⁻¹) ^b
Holland 2014 ⁷	0.5	720	80	not listed	88 ^c	1:5.3	>0.24
limited functional group tolerance							
Hilt 2015 (Co) ^{8a}	10	90	rt	95	92 ^d	1:5.6	0.11
Hilt 2015 (Ni) ^{8b}	10	360	-60	90	72 ^e	1:2.6	0.025
catalysts made from Ph ₂ PH, Zn, ZnI ₂ , and MX ₂ (dppb); Ni catalyst selectivity erodes at higher temperatures							
Dobereiner 2018 ⁹	0.5	30	66	94	92 ^c	1:4.0	6.3
fast, good functional group tolerance, but slower in their presence and with longer alkenes							
Grotjahn 2007 (1)	0.1	15	rt	98	86 ^c	>99:1	65
fast, excellent (<i>E</i>)-selectivity; lower positional selectivity							
Grotjahn 2014 (2+2a)	1	2880	40	98	96 ^c	>99:1	0.034
excellent (<i>E</i>)- and monoselectivity, but slow							
Huang 2017 ¹¹	0.1	480	rt	96	95 ^c	25:1	2.0
fast, very (<i>E</i>)- and monoselective; alkenes distilled from LiAlH ₄ in many cases							
this work (5)	0.1	180	rt	98	97 ^c	>400:1	5.4
fast, very (<i>E</i>)- and monoselective, good functional group tolerance							

^aAll reactions were run between 0.5–1.0 M in substrate. ^bCalculated with conversions at indicated time point without factoring temperature. ^c2-Hexene. ^d2-Hexadecene. ^e2-Decene.

1). In 1988, Tilley and Chaudret independently discovered the pioneer complexes $\text{Cp}^*\text{Ru}(\text{PR}_3)\text{Cl}$, where $\text{R} = \text{iPr}$ or Cy . $\text{Cp}^*\text{Ru}(\text{L})\text{X}$ complexes have been synthesized by complexation of PR_3 with either Cp^*RuCl_4 ¹⁴ or a mixture of Cp^*RuCl_2 dimer and Zn .¹⁵ A striking feature of both reported complexes is their blue color both in solution and in the solid state, contrasting with yellow to orange color of 18-electron $\text{CpRu}(\text{II})$ species mentioned here in this article. It has been suggested that the blue color in these and subsequent $\text{Cp}^*\text{Ru}(\text{P})\text{X}$ complexes is the result of π -donation of a lone pair from the halide to the metal center, which stabilizes a formally 16-electron state.¹⁶

After Tilley's and Chaudret's initial discoveries, several 16-electron complexes of the general formula $\text{Cp}^*\text{Ru}(\text{L})\text{X}$ could be accessed if L was a bulky phosphine ligand with the general formula $\text{P}(\text{R}^1)_2(\text{R}^2)$, where R^1 was isopropyl or cyclohexyl and where X was either a halide^{16–19} or a weakly basic oxygen-containing X -type ligand such as triflate, $\text{Ph}_3\text{SiO}-$, or $\text{CF}_3\text{CH}_2\text{O}-$.^{16,20,21} We reasoned that the Cp^*RuCl fragment could therefore accommodate the (diisopropyl)(imidazolyl)phosphine ligand employed in catalysts **1** and **2**, although it was not clear whether the ligand would bind in a monodentate fashion to produce a 16-electron complex akin to Tilley and Chaudret's examples or would chelate through the imidazole as well to produce an 18-electron complex. Because the switch of the Cp ligand in catalyst **1** to the bulkier and more electron-rich Cp^* ligand in catalyst **2** + **2a** engendered an increase in monoselectivity, we wondered whether steric or electronic factors lead to the change. We therefore made **4** (and ultimately **6**) with the more electron-poor tetramethyl-(trifluoromethyl)cyclopentadienyl (Cp^\ddagger) ligand, which has been shown to mimic the sterics of Cp^* and the electronics of Cp .^{22,23}

Complexation of the requisite phosphine with $[\text{Cp}^*\text{RuCl}]_4$ or $[\text{Cp}^\ddagger\text{RuCl}]_4$ occurs efficiently in solvents such as acetone and THF with a rapid change in color of the solution from deep red to deep blue. The blue color is reminiscent of many Cp^*Ru 16-electron complexes, and NMR data for the major species (>90% by ³¹P NMR) are also consistent with the formally 16-electron species $\text{Cp}^*\text{Ru}(\text{L})\text{Cl}$ (**3**, Cp^* and **4**, Cp^\ddagger). There is some evidence of equilibrium between these monomeric species and related tetrameric species (see Figures S9–S18 and the discussion in the Supporting Information). The isopropyl group signals in the ¹H NMR spectra of **3** and **4** appear as a pair of dd, suggesting a symmetrical static structure such as that drawn in Scheme 1; alternatively, if solvent is bound, forming an 18-electron species, the association of solvent is weak. The ¹⁵N HMBC chemical shift of the basic nitrogen of the imidazole in **3** ($\delta^{15}\text{N} -100.6$ ppm, Table 2) is consistent with an unchelated imidazolylphosphine,²⁴ as is the coupling constant for the phosphorus to the C-2 of the imidazole ($^1J_{\text{CP}} = 51.9$ Hz). Complexes **2** + **2a** can be used as comparisons for the $^1J_{\text{CP}}$ coupling constant, as both chelated (**2**) and unchelated (**2a**) forms of the complex exist. The $^1J_{\text{CP}}$ in **3** much more closely resembles that in **2a** (58.0 Hz) rather than that in **2** (28.6 Hz).¹⁰ The large C-2 coupling constant for complex **4** ($J = 43.7$ Hz) also suggests a lack of chelation and hence 16-electron character.

Prolonged storage in cyclohexane at -40 °C gave crystals of **3** suitable for X-ray diffraction. The crystal structure of **3** (Figure 1, Table 3) shows a two-legged piano-stool structure characteristic of 16-electron Cp^*Ru complexes with $\text{P}(1)$, $\text{Cl}(1)$, and $\text{Ru}(1)$ coplanar with the Cp^* centroid. Consistent

Table 2. $^1J_{\text{C-P}}$ (Hz) and ¹³C and ¹⁵N Chemical Shifts (ppm)^a

complex	Im–C1		N(2)	N(1)–CH ₃
	¹³ C chemical shift	<i>J</i>	¹⁵ N chemical shift	¹⁵ N chemical shift
2	142.5	58.0	n.d.	n.d.
2a	148.3	28.5	n.d.	n.d.
3^{b,c}	141.9	51.9	–100.6	–213.1
4	146.0	43.7	–136.2	–213.7
5^{b,d}	152.0	19.3	–147.0	–203.1
6^{b,d}	151.9	21.7	–155.7	–204.5
7^d	146.5	34.7	n.d.	n.d.
8^d	152.5	24.1	–164.3	–210.2
9	152.6	22.1	–158.3	–203.7
10	152.3	25.2	–168.8	–205.1

^aData for **2** and **2a** are from literature.¹³ n.d. = not determined. ^b16-Electron crystal structure. ^cN(2) unbound to Ru in the crystal structure. ^dN(2) bound to Ru in the crystal structure.

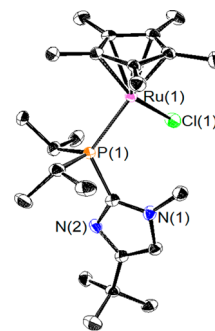


Figure 1. X-ray crystal structure of complex **3**. Key bond lengths (Å) with values for each independent molecule in the unit cell: Ru–P, 2.3582(13) and 2.3699(13); Ru–Cl, 2.703(12) and 2.3591(12); Ru–Cp(centroid), 1.772 and 1.780, respectively.

with the HMBC data, the basic N(2) shows no interaction with ruthenium, in contrast to **2** and to other systems containing Cp^*RuCl metal fragments with a P–N ligand. The P–N ligands $\text{iPr}_2\text{P-2-dimethylaminoindenide}$ studied by Stradiotto,²⁵ $\text{Ph}_2\text{P}(\text{CH}_2)_2\text{NMe}_2$ by Kirchner,²⁶ and $\text{Ph}_2\text{P}(\text{CH}_2)_2\text{NH}_2$ by Ikariya^{27–29} were shown to chelate through both the phosphorus and nitrogen to Cp^*RuCl , leading to 18-electron complexes. All three published systems feature a P–C–C–N–Ru five-membered chelate. From our lab, cationic species **2** features a 4-membered chelate. We have shown previously in an alkyne hydration catalytic system with a pyridyl-phosphine ligand that the introduction of a *tert*-butyl group adjacent to the nitrogen can greatly enhance the hemilability of the chelate.²⁴ We presume that the steric and angle strain combined with the strong π -donation of the halide prevents chelation from occurring in **3** and **4**.

To examine this further, complexes **7** and **8**, lacking the *tert*-butyl group, were generated from the appropriate tetramer and phosphine. Although some evidence for 16-electron species, or at least rapid hemilability of the chelate, is presented in solution (blue color for **7**, symmetry in ¹H NMR for **7** and **8**), X-ray crystal structures for **7** and **8** feature a chelated nitrogen (Figure 2). The chelate lengthens the Ru–Cl bond of **7** as compared to **3** (2.47 Å vs 2.36 Å), which could be ascribed to lack of Ru–Cl multiple-bond character for **7**.

The mixture containing complex **3** was tested for isomerization under similar conditions as those for **2** + **2a** but was

Table 3. X-ray Crystal Structure Data

compound	3	5	6	7	8	[Cp ⁺ RuCl] ₄
formula	C ₂₇ H ₄₉ ClN ₂ PRu	C ₂₄ H ₄₂ F ₆ N ₂ P ₂ Ru	C ₂₄ H ₃₉ F ₉ N ₂ P ₂ Ru	C ₂₀ H ₃₄ ClN ₂ PRu	C ₂₀ H ₃₁ ClF ₃ N ₂ PRu	C ₄₀ H ₄₈ Cl ₄ F ₁₂ Ru ₄
formula weight	569.17	635.60	689.58	469.98	523.96	1302.86
crystal system	tetragonal	orthorhombic	monoclinic	monoclinic	monoclinic	triclinic
space group	P4 ₁	Pna21	P21/c	P21/c	P21/c	P1
crystal color	blue	blue	blue	orange	orange	red-orange
unit cell parameters (lengths in Å, angles in °)	$a = 13.2477(9)$ $b = 13.2477(9)$ $c = 32.6230(2)$ $\alpha = 90$ $\beta = 90$ $\gamma = 90$	$a = 22.7385(8)$ $b = 13.1551(5)$ $c = 9.5634(3)$ $\alpha = 90$ $\beta = 90$ $\gamma = 90$	$a = 22.5581(7)$ $b = 12.7798(4)$ $c = 22.1335(7)$ $\alpha = 90$ $\beta = 113.1800(10)$ $\gamma = 90$	$a = 13.3641(6)$ $b = 15.0206(7)$ $c = 10.9602(6)$ $\alpha = 90$ $\beta = 93.975(2)$ $\gamma = 90$	$a = 13.915(3)$ $b = 14.954(4)$ $c = 10.922(3)$ $\alpha = 90$ $\beta = 95.212(6)$ $\gamma = 90$	$a = 11.6853(6)$ $b = 20.7278(10)$ $c = 21.1082(10)$ $\alpha = 114.576(2)$ $\beta = 96.8470(10)$ $\gamma = 99.3550(10)$
temperature (K)	100.0	100(2)	100.0	100.0	100.0	100
Z, Z'	8	4	8, 2	4	4	4
R ₁ (obs)	0.0312	0.0675	0.0372	0.0501	0.0384	0.0285
wR ₂ (all)	0.0724	0.1768	0.1040	0.1120	0.0756	0.0661
GOF	1.025	1.218	1.029	1.032	1.012	1.033
				final R indices		

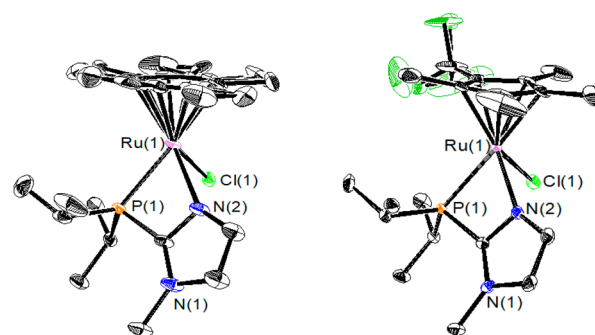


Figure 2. X-ray crystal structure of complexes 7 and 8. Key bond lengths (Å) and angles (deg): 7: Ru–P, 2.3906(10); Ru–N, 2.203(4); Ru–Cl, 2.4713(10); Ru–Cp(centroid), 1.779; P–Ru–N, 66.94(10). 8: Ru–P, 2.3925(9); Ru–N, 2.185(2); Ru–Cl, 2.4595(8); Ru–Cp(centroid), 1.780; P–Ru–N, 66.92(7).

found to be a very poor catalyst (<1 turnover in 1 week). There could be several reasons for the sluggish catalysis: (1) the halide is too strong of a π -donor, thereby inhibiting binding of the alkene to the metal center; (2) the neutral charge of the complex disfavors binding of the alkene or formation of a formally anionic allyl ligand that we have previously proposed as an intermediate during catalysis; or (3) the monodentate phosphine provides more steric demand due to free rotation of the Ru–P and P–C(imidazolyl) bonds. To address all three reasons, the mixture containing 3 was treated with TIPF₆ to make a cationic complex (5) in acetone, which was obtained in 98.2% yield.³⁰ 4 was converted to 6 in the same fashion.³¹

We expected that upon ionization and halide ligand loss from 3, the cationic complex would bind the imidazole nitrogen as well as another solvent molecule to produce an 18-electron complex due to the removal of the π -stabilizing chloride ligand. A significant upfield shift of the ¹⁵N HMBC resonance for the basic imidazole nitrogen ($\delta_N = -147.0$ ppm, Table 2) occurs, which brings it within the range for P,N-chelated imidazolyl phosphine ligands.²⁴ However, the ¹H NMR spectrum shows sharp peaks for all resonances with one septet of doublets (2H) for the isopropyl C–H protons and two dd (each 6H) for the isopropyl-CH₃ protons, suggesting planar symmetry¹⁶ or fast reversible binding of solvent molecules to the metal center.³² However, no broadening of the ¹H signals occurred, nor did we observe new signals (for either bound acetone or desymmetrization of the phosphine ligand) consistent with binding of acetone upon cooling the solution to -30 °C.

Surprisingly, the color of the solution upon ionization remains deep blue; UV–vis spectroscopy shows a large broad absorption centered around 572 nm ($\epsilon = 748$ L/mol·cm). The combination of spectroscopic data point to the persistence of a 16-electron complex despite the removal of the halide ligand. The blue color remains upon removal of solvent, and the intensely blue powder is stable for months under air-free conditions. Solutions of 5 can be made with undried acetone, which can maintain their color and activity for a few days.

Crystals suitable for X-ray diffraction of 5 and 6 were grown by vapor diffusion of diethyl ether into acetone. In the solid state, complexes 5 and 6, like 3, exhibit planar symmetry with P(1), N(2), and Ru (1) coplanar with the Cp centroid (Figure 3). No solvent molecules are coordinated, and there are no C–H bonds close enough to the metal center to participate in agostic interactions with the closest M–H interaction being

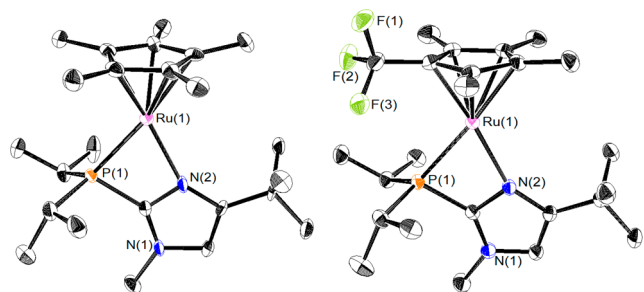


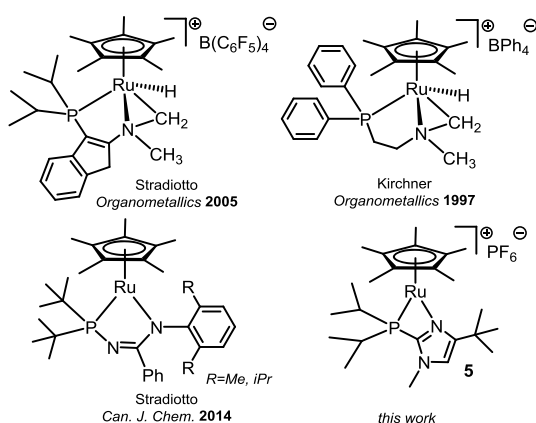
Figure 3. X-ray derived molecular structures of the cations in complexes **5** and **6** (PF_6^- anions omitted). Key bond lengths (Å) and angles (deg) with values for each independent molecule in the unit cell: **5** (one molecule in unit cell): Ru–P, 2.386(2); Ru–N, 2.242(10); Ru–Cp(centroid), 1.773; N–Ru–P, 68.3(2). **6** (two molecules in unit cell): Ru–P, 2.3905(6) and 2.3930(6); Ru–N, 2.1501(18) and 2.1599(18); Ru–Cp(centroid), 1.775 and 1.773; N–Ru–P, 69.00(5) and 68.92(5), respectively.

between one of the methyl groups of an isopropyl with M–H distances 3.0 Å for **5** and 3.1 Å for **6**.

$\text{Cp}^*\text{Ru}(\text{P–P})^+$ and $\text{Cp}^*\text{Ru}(\text{N–N})^{+/0.33-3.5}$ 16-electron complexes have been well-studied. In the absence of coordinating solvent molecules, agostic C–H bonds or even trace amounts of dinitrogen are known to lead to 18-electron complexes,³⁶ so to make mono- and bidentate cationic $\text{Cp}^*\text{Ru}(\text{PP})$ complexes, ionizations were performed with fluorobenzene under argon.^{19,25} Related 16-electron N–N chelates appear to be more stable due to strong σ -donation.

Although Cp- and $\text{Cp}^*\text{Ru}(\text{P–N})$ systems have been shown by Stradiotto, Ikariya, and our group to be effective catalysts for alkyne hydration, alkene hydrosilylation,³⁷ alkene isomerization,^{10,24,38–41} and hydrogenation of ketones, epoxides,²⁷ imides,⁴² esters, and carboxamides,⁴³ well-defined, formally unsaturated $\text{Cp}^*\text{Ru}(\text{P–N})$ complexes are quite rare; several reported in the literature exhibit characteristics of 16-electron species but cannot be isolated because of chemical instability. Stradiotto observed that upon abstraction of the halide from the $\text{Cp}^*\text{Ru}(\text{iPr}_2\text{P-2-dimethylaminoindenide})\text{Cl}$ complex, either oxidative addition of one of the methyl C–H bonds or arene complexation occurred (Chart 2), although a 16-electron intermediate was suggested.^{25,37,44} Similarly, Kirchner observed oxidative addition of a methyl C–H bond.²⁶ These transformations could be facilitated by the removal of the stabilizing π -donation afforded by the chloride ligand. The

Chart 2. Known $\text{Cp}^*\text{Ru}(\text{PN})$ Complexes



closest comparison structurally to **5** is a pair of complexes from Stradiotto, $\text{Cp}^*\text{Ru}(\text{t-Bu}_2\text{P–N-amidinate})$ complexes⁴⁵ that contain chelating anionic phosphine-amido ligands (Chart 2). To the best of our knowledge, **5** is the first reported example of a fully characterized, cationic $\text{Cp}^*\text{Ru}(\text{P–N})$ 16-electron complex, and **6** is the first reported 16-electron Cp^*Ru phosphine complex of any kind.

Catalysis Scope and Limitations. As hypothesized, **5** proved to be an exceedingly efficient catalyst relative to its nitrile-containing counterpart (Table 4). Isomerization reactions of linear 1-alkenes to (*E*)-2-alkenes using catalyst **5** can be performed at room temperature in acetone- d_6 using as little as 0.1 mol % catalyst and reach full conversion within 3 to 4 h at this low loading (Table 5). In several cases, alkene samples could be used as received once deoxygenation was performed by bubbling nitrogen gas through the alkene substrates prior to use. However, we suspect that trace impurities of allylic peroxides in some of the alkene substrates lead to significant deactivation of the catalyst at 0.1 mol % loadings. One solution is pretreatment of the substrate by passing it through a small plug of basic alumina. At catalyst loadings of ≥ 0.5 mol %, this pretreatment was not necessary, and most substrates underwent complete isomerization within 15 min to 1 h. In addition to the alkenol and alkenol silyl ether substrates reported for **2** + **2a**,¹⁰ we show that protected amide and ester substrates are tolerated and isomerize efficiently at 1.0 mol %. In all cases with conversions of starting 1-alkene at 95% or greater, yields of (*Z*)-alkenes were less than 0.5%, and yields of 3-alkenes were less than 3%, showing remarkable general selectivity for formation of (*E*)-2-alkene products (Table 5).

To investigate the relative efficiency of **5** to the mixture of **2** + **2a**, we compared the half-life of conversion of 1-hexene to (*E*)-2-hexene at room temperature using 0.25 mol % of each catalyst. We found that while catalyst **2** + **2a** reached $\sim 50\%$ conversion after 40 h, catalyst **5** reached 50% conversion in only 5.6 min, making it >400 times faster at synthetically reasonable loadings. The increase in efficiency can be directly attributed to the lack of acetonitrile; in an attempt to mimic the **2** + **2a** system, 1.7 equiv of acetonitrile was added to a solution of **5** and run with the same 0.25 mol % at room temperature and achieved only 38% conversion after 48 h.

A major advantage that catalyst **5** has over **2** + **2a** is its ability to isomerize substrates that contain potentially strongly binding or chelating functional groups, which can slow catalysis. **2** + **2a** (1 mol %, 40 °C, 48 h) was able to isomerize the *tert*-butyldiphenylsilylether of pent-4-en-1-ol to provide $>90\%$ yield of the (*E*)-2-isomer but required 6 mol % extra phosphine ligand to prevent catalyst deactivation by way of an arene complex.¹⁰ With the same substrate, catalyst **5** still suffered from arene complex formation, but due to its greater efficiency, 1 mol % **5** can achieve $>95\%$ yield of the (*E*)-2-isomer within 10 min with no added ligand. This result opened the door to testing other substrates containing phenyl groups; 9-phenyl-1-decene was isomerized smoothly with 1 mol % **5**, as was the phenylbutene discussed below.

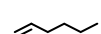
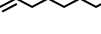
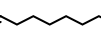
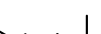
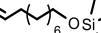
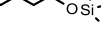
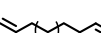
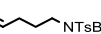
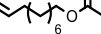
Terminal alkene substrates containing unsaturated moieties in the 5-position present an interesting thermodynamic challenge for catalyst **5**. In these substrates, if a double bond is isomerized once, the resulting product is not conjugated, but if a second isomerization occurs, the result is a conjugated π -system that provides significant extra stability over the unconjugated isomer. For example, an equilibrium mixture of 1-phenylbutenes, established between 25 and 55 °C, gave

Table 4. Isomerization of 1-Hexene with 1, 2, 5, and 6^a

catalyst	mol %	time	1-hexene	(E)-2-hexene	(E)-3-hexene	TOF (min ⁻¹) ^d
1	0.1	15 min	2	86	11	65
		20 min	2	79	20	49
2 + 2a ^{b,c}	1	48 h	2	96	2	0.034 ^e
5	0.1	3 h	2	97	1.5	5.4
6	0.1	32 h	2	97	0.7	0.51

^aReactions were run at 0.50 M in acetone-*d*₆ with internal standard. ^bReaction was run at 40 °C. ^cFrom ref 10. ^dCalculated with conversions at the indicated time point. ^eTOF at 40 °C.

Table 5. Alkene Yields (%) and E/Z Selectivity Using Catalyst 5^a

Entry	Substrate ^a	Mol % 5	Time (min)	Conv.	(E)-2-	(E)-2/ (Z)-2 ^b	(E)-3-
1		0.1	180	98	97	>400:1	1
2 ^d		0.5	20	98	97	>400:1	1
3		0.5	30	98	96	>200:1	2
4		0.1	240	98	96	>400:1	2
5		0.5	30	98	94	>400:1	3
6		0.1	240	98	96	>400:1	2
7 ^d		0.5	20	98	96	>400:1	2
8 ^d		0.5	30	99	99	>200:1	<0.5
9		0.5	45	97	97	>400:1	<0.5
10		0.5	15	98	96	>200:1	2
11 ^d		0.5	15	97	96	n.d. ^c	1
12		0.5	15	97	97	n.d.	n.d.
13		0.5	15	98	97	89:1	1
14		1.0	10	96	95	>400:1	1
15		1.0	15	97	96	>50:1	1
16		1.0	40	96	95	n.d.	0.3
17		1.0	30	97	95	>400:1	2
18		1.0	240	88	66	>400:1	22
19 ^d		1.0	40	95	92	>400:1	3
20 ^d		0.5	120	97	93	>100:1	3
21		2.0	10	>97	>94	n.d.	0.4

^aReactions were run at room temperature with 0.50 M substrate in acetone-*d*₆. ^bConservative estimates; for in-depth analysis, see Figures S46–S66 and Tables S6 and S7. ^cn.d. = not determined because of either signal overlap or broadness. ^dReactions were run in triplicate.

ratios of conjugated 1-phenyl-(E)-2-butene to unconjugated 1-phenyl-(E)-3-butene that ranged from 92:6 to 94:3.^{46–48} Similarly, an equilibrium mixture of hexenones was reported to contain ~16% unconjugated hex-(E)-4-en-2-one, ~7% conjugated hex-(Z)-3-en-2-one, and ~77% conjugated hex-(E)-3-en-2-one.⁴⁹ If the ratios are recalculated excluding the (Z)-isomer, the ratio becomes 83:17 in favor of the conjugated (E)-isomer.

Given the strong thermodynamic preference for the conjugated internal isomer, a true challenge for catalyst 5 is the isomerization of the terminal alkene substrates for these two systems: 5-hexen-2-one (Table 5, entry 18) and 1-phenyl-4-butene (Table 5, entry 19). 1,2-Epoxy-5-hexene (Table 5, entry 20) and 1,7-octadiene (Table 5, entry 21), are also prone to overisomerization: in the former case, an internal conjugated diene can result, and in the latter case, using 1, we have observed ring opening and conjugated enal formation.⁵⁰

Higher catalyst loadings are ultimately required for the diene, enone, and phenyl substrates, likely due to chelation or deactivation of the catalyst via arene complex formation. The results for 1-phenyl-4-butene are striking (Table 5, entry 19): catalyst 5 can achieve a 91.9:4.3 ratio of unconjugated and conjugated products, the complete opposite of the thermodynamic ratio mentioned above. Overisomerization at later times was slow likely due to catalyst deactivation by arene complexation. Selective monoisomerization was also seen with 1,2-epoxy-5-hexene (Table 5, entry 20) with very little enal formation due to the deactivation of catalyst by decarbonylation of the aldehyde.⁵⁰ In entry 18, 5-hexen-2-one suffers from more rapid overisomerization⁵¹ with a maximum yield of monoisomerized product at 66% at 4 h, but monoisomerization is still favored over conjugation by around 3:1 at this point. The conversion of 1,7-octadiene to (2E,6E)-2,6-octadiene requires the migration of two separate double bonds; nevertheless, with higher 2 mol % loading, the doubly monoisomerized product yield reaches >94% within 10 min, but the conjugated diene does not appreciably increase within 24 h.

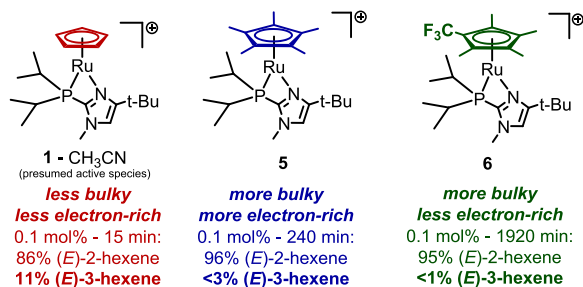
Sterics or Electronics? The pentamethylcyclopentadienyl (Cp*) ligand is both more electron-rich and sterically bulky than the cyclopentadienyl (Cp) ligand.^{52,53} Given the distinct differences in reactivity between Cp-containing catalyst 1 (which is fast but not positionally selective) and Cp*-containing 2 + 2a and 5 (which are selective for monoisomerization), we wanted to investigate whether the change in selectivity during catalysis is the result of steric or electronic influences between the Ru center and the alkene. Catalytic and structural comparisons between Cp- and Cp*Ru complexes^{54–60} have been undertaken, employing the 1-(trifluoromethyl)-2,3,4,5-tetramethylcyclopentadienyl (Cp[‡]) ligand developed by Gassman,²² reported to mimic the

electronics of the Cp ligand and sterics of the Cp* ligand.^{22,23,61}

To obtain the Cp[†] analogue (6) of catalyst 5, the [Cp[†]RuCl]₄ tetramer was first prepared following a protocol by Evju and Mann⁶² in which they speculated the tetramer had formed during the synthesis. The [Cp[†]RuCl₂]₂ dimer was reduced with Zn metal in refluxing methanol; the tetramer was isolated in 91% yield, characterized, and a crystal structure was obtained (see Figure S3). The requisite phosphine was added to [Cp[†]RuCl]₄, leading to complex 4, which was cleanly ionized with TlPF₆ to obtain complex 6 in 94% yield. The crystal structure of 6, like that of 5, shows a cationic, formally 16-electron species. A comparison of the structures reveals similarities: Ru–P bond distance is essentially identical (2.386(2) Å for 5, 2.3905(6) Å for 6) as is the distance from the metal center to the Cp centroid (1.773 Å for 5, 1.775 Å for 6), both well within the margin of error. However, the Ru–N distance in 6 (2.1501(18) Å) is almost 0.1 Å shorter than that in 5 (2.242(10) Å). This is perhaps a consequence of the nitrogen being directly trans to the carbon containing the –CF₃ group in the crystal structure.

Albeit slower than 5, complex 6 is also able to cleanly isomerize 1-hexene to >95% (*E*)-2-hexene using 0.1 mol % catalyst after 32 h. Because the alkene isomerization positional selectivity more closely aligns with that of catalyst 2 + 2a and 5 than that of 1 (Chart 3 and Table 4), it can be inferred that the

Chart 3. Steric and Electronic Influences on Selectivity



selectivity for monoisomerization for catalysts 2 + 2a and 5 is a result of increased steric bulk of the Cp* ligand rather than its increased electron-donating ability. Despite the comparable selectivity of 6 and 5, the lower rate of the former makes 6 a rather inferior choice for practical use. A hypothesis for why 6 is slower than 5 is discussed below.

Bonding and Stability in 16e⁻ Complexes 5 and 6.

The major increase in activity of catalyst 5 over 2 + 2a clearly results from an open coordination site and the lack of the competitive nitrile ligand for the alkene. An intriguing question arises as to why the catalyst is stable enough to be isolable in the solid state and in weakly binding solvents such as acetone and THF yet reactive enough to efficiently isomerize terminal alkenes. To probe this question, a computational study was undertaken to analyze the orbitals involved in stabilization of the 16-electron species. The WB97XD functional with an SDD basis set with effective core potential was used for ruthenium, and the cc-pVDZ basis set was used for all other atoms after benchmarking with experimental data for Ru–N and Ru–P bond distances, NMR, and UV–vis (see Tables S71–S79 on pages S234–S238 in the Supporting Information for details).

An analysis of the relevant molecular orbitals with π -symmetry between the ruthenium and chloride in complex 3

reveals four MOs with π -bonding character (HOMO–9, HOMO–8, HOMO–7, and HOMO–5) and three MOs that are antibonding (HOMO–2, HOMO–1, and HOMO) with respect to the two atoms, resulting in one “net” π -bond. The LUMO is also antibonding with π -symmetry with respect to ruthenium and chloride. A similar bonding scenario can be seen when we subjected Tilley and Chaudret’s Cp**Ru*(iPr₃P)–Cl complex to the same computational analysis (see Table S86) and is consistent with other analyses of Cp**Ru*(PR₃)X systems.

Upon abstraction of the halide from 3 and 4 to form complexes 5 and 6, respectively, crystal structure and NMR data are consistent with a two-legged piano stool complex with planar symmetry, similar to 3 and other formally 16-electron complexes. The computed molecular orbitals for complexes 5 and 6 indicate a similar π -stabilizing interaction. For complex 5, the HOMO–7 (Figure 4) represents a π -bonding

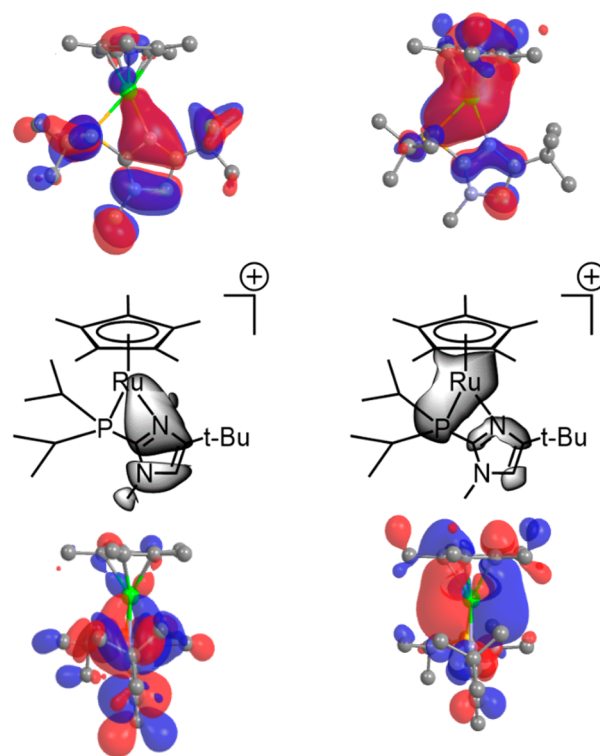


Figure 4. Computed molecular orbitals for complex 5. Top left: HOMO–7 (face view). Middle left: ChemDraw of HOMO–7 (face view). Bottom left: HOMO–7 (edge view). Top right: LUMO (face view). Middle right: ChemDraw of LUMO (face view). Bottom right: LUMO (edge view).

interaction between the coordinated basic nitrogen and the two neighboring carbons of the imidazole and the metal center. This bonding MO resembles a filled molecular orbital on the free ligand and a large majority of its contribution and can therefore be assigned as a ligand-to-metal π -donation. For complex 6, the HOMO–8 is a similar π -type bonding orbital, albeit with the electron density shifted from the C4 carbon toward the phosphorus atom, which contributes 19% toward the bonding orbital as opposed to only 3% for 5.⁶³ The π -donation shown from the imidazole provides the metal with the missing two electrons from the formal 16-electron assignment to generate an electronically saturated complex in a similar fashion to the Cp**Ru*(PR₃)X (where X = Cl, Br, I,

OR, NR)^{16,21,45,64} but differs in that the donation originates from a π -system on the imidazole rather than a lone pair on an anionic X atom. While π -donation is not needed to generate a 16-electron cationic Cp*Ru species, as seen with Cp*Ru(P–P)⁺ and Cp*Ru(N–N)⁺ complexes, the competent π -donating ability of imidazole^{65,66} likely leads to a higher level of stability for complexes **5** and **6**.

It should be noted that the bulk of the *tert*-butyl group on the *N*-methyl-4-*tert*-butylimidazole moiety also contributes to the persistent 16-electron nature of **5** and **6** in solution. Complexes **9** and **10**, formed by ionization of **7** and **8**, respectively, lack the *tert*-butyl group. Although the ¹H NMR spectra of **9** and **10** also appear symmetrical at room temperature, they lack the characteristic blue color that is prevalent in the 16-electron Cp*Ru complexes and likely undergo rapid reversible binding of solvent. Whether the difference in behavior is due to steric or electronic properties of the *tert*-butyl group is not clear.

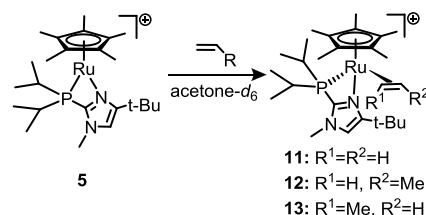
The LUMO of complexes **5** and **6**, on the other hand, is antibonding with respect to the ruthenium and the π -system of the imidazole, much like in complex **3**. The LUMO resides mostly on the ruthenium (56% for both **5** and **6**), suggesting that if an incoming ligand binds to the metal and its electrons populate the LUMO, the π -bonding interaction could be severed to establish a coordinatively saturated complex that retains its 18-electron count. The flat and diffuse shape of the LUMO appears to be ideal to accommodate the π -orbital of an alkene as opposed to a lone pair on a solvent molecule. Evidence of the alkene–metal LUMO interaction for catalyst **5** can be seen in the spectrometric changes that occur upon addition of alkenes to solutions of the catalyst, which can provide direct indications of the behavior for isomerization with **5**.

Studies of Alkene Binding. Using NMR and UV–vis spectroscopies, clear evidence of alkene binding can be seen with small alkenes such as ethylene and propylene, providing insights into the structure of alkene complexes formed using complex **5**. Furthermore, the interaction of hexene isomers with **5** provides compelling insight into the selectivity of isomerization.

Binding of Ethylene. The most prominent feature of a UV–visible spectrum of catalyst **5** is a broad, intense absorbance with a maximum of 582 nm, which is responsible for its deep blue color. Time-dependent density functional theory calculations of the complex ascribe this absorbance to two major transitions: HOMO→LUMO and HOMO–1→LUMO, which are both metal-to- π^* (Ru–imidazole) transitions. If the LUMO is populated by an incoming ligand such as an alkene, the transitions should be quenched, and the blue color should diminish as the complex attains 18 electrons. These changes are clearly observed when ethylene is bubbled through a solution of **5**: the solution changes color from deep blue to a light yellow, and there is almost complete bleaching (96% reduction) of the absorbance at 582 nm.

¹H NMR data for the species formed from **5** and ethylene are fully consistent with structure **11** (Scheme 2), which is an 18-electron complex containing a single bound ethylene. In the ¹H NMR spectrum, the ethylene signal is visible as a broad signal centered at 2.45 ppm. When the sample is cooled to –30 °C, 4 separate ethylene C–H signals are visible, ranging from 2.1 to 3.5 ppm, which become sharper upon further cooling. Two isopropyl C–H and four isopropyl-CH₃ peaks are also

Scheme 2. Reactions of **5** with Ethylene and Propylene



resolved, consistent with four unique methyls in **11** and strongly implicating one ethylene and chelated PN ligand.

Binding of Propylene Forming Two Diastereomers. When propylene is introduced to a solution of **5**, the blue color lightens considerably, and NMR data at low temperatures (≤ -30 °C) are consistent with a mixture of two diastereomers, **12** and **13** (Scheme 2), as the major species in a roughly 4:1 ratio. Signals corresponding to the minor diastereomer are broader but become sharper around –60 °C. For the two major species, at all temperatures, the imidazole C–H signal in the ¹H NMR spectra as well as the singlet in ³¹P NMR spectra shift upfield relative to those of complex **5**; moreover, the isopropyl C–H protons appear as two distinct signals, signifying a desymmetrization of the complex consistent with binding of the propylene. In addition, between –40 and –60 °C, 3 additional signals in ¹H NMR spectra begin to resolve (one broad and two doublets) between 2.5 and 3.8 ppm that integrate to one proton each for the major species. These new signals could represent the alkene C–H peaks for bound propylene, although no crosspeaks are observed between these signals in 2D COSY NMR spectra. To obtain definitive evidence for alkene binding in both diastereomers, a mixture of triply labeled (¹³C)₃-propylene and **5** was prepared. Figure 5

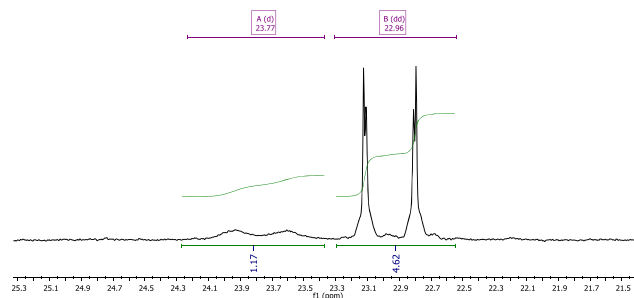


Figure 5. Signals assigned to the methyl of bound propene in **12** and **13**. Shown is the aliphatic region (21 to 25 ppm) of the ¹³C NMR spectrum (150.7 MHz, acetone-*d*₆) of a solution of (¹³C)₃-propylene and **5**.

shows the ¹³C NMR signals for the carbon of the –CH₃ group (R¹ or R² in Scheme 2) for bound propylene. The larger, upfield signal at 22.9 ppm is roughly four times larger than the broader downfield signal at 23.8 ppm (and the methyl group for free propylene appears at 19.7 ppm).

Binding of Hexene Isomers and Their Transformation. For **5** to accomplish (*E*)-selective monoisomerization of most alkene substrates, the rate of isomerization of 1- to (*E*)-2-alkene must be much higher than that of the (*E*)-2- to (*E*)-3-alkene transformation. The kinetic preference of the first isomerization over the second could be linked to either binding/release of the alkene from the catalyst or an

intermediate step in the mechanism, or both. Both NMR and UV–visible spectroscopy allow characterizing the binding of catalyst and hexene isomers, elucidating binding contributions to selectivity, and potentially identifying steps in the catalytic cycle.

The visible behavior of the catalyst in the presence of larger isomerizable alkenes such as 1-hexene is more complex than when ethylene is present. When the isomerization of 1-hexene is performed with catalyst **5**, the solution is initially lighter in color but still retains a blue coloration. As the reaction proceeds, the blue color deepens, typically reaching its maximum when the 1-hexene amount is minimized. When the reaction was observed using UV–vis spectroscopy (Figure 6, top), a significant drop in the absorbance at 582 nm occurs

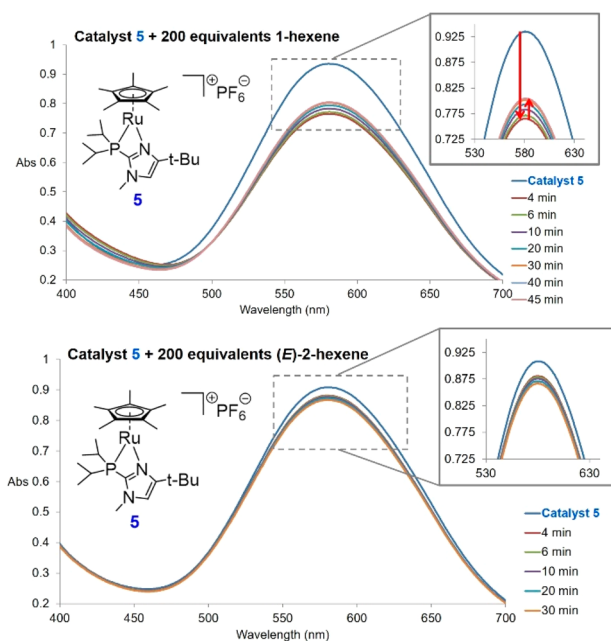


Figure 6. UV–visible spectra of **5** before and after addition of hexenes. Top: **5** with 200 equiv of added 1-hexene monitored every 2–10 min. Bottom: **5** with 200 equiv of added (*E*)-2-hexene monitored every 2–10 min, starting 4 min after addition.

when 1-hexene is introduced, and then throughout the course of the next 30 min, the intensity of the absorbance partially recovers.

We attribute the initial decrease in absorbance to binding of 1-hexene to the complex, which populates the LUMO and quenches the metal-to-LUMO transition and therefore the absorbance at 582 nm, as was the case with ethylene. As the 1-hexene is consumed, the absorbance intensity partially returns, suggesting an increase in amount of free complex (Figure 6 top); we hypothesize that the (*E*)-2-hexene product does not bind as favorably as 1-hexene to the catalyst. Further evidence for the hypothesis is that in a separate experiment, addition of (*E*)-2-hexene to a solution of **5** produces essentially no drop in absorbance (Figure 6 bottom). A scenario in which 1-hexene binds to catalyst to a greater extent than (*E*)-2-hexene may explain why **5** isomerizes 1- to (*E*)-2-hexene faster than (*E*)-2- to (*E*)-3-hexene. Significantly, the fact that ethylene completely bleaches the 582 nm absorbance whereas 1-hexene reduces the absorbance by only ~20% after 4 min suggests strongly that significant amounts of catalyst remain uncomplexed even in the presence of 200 equiv of 1-hexene.⁶⁷

While UV–vis spectroscopy illustrates differences between the interactions of 1- and (*E*)-2-hexene with **5**, NMR spectroscopy should allow for simultaneous determination of both catalyst and alkene concentrations. As detailed below, we are unable to identify signals for *bound* hexene in the NMR spectra, but fortunately, we can use readily identifiable catalyst-derived signals assigned to alkene complexes and large signals for *free* alkene. Changes in the intensity and position of catalyst-derived signals provide useful information on relationships between catalyst, alkenes, and alkene complexes. Careful ¹H NMR spectroscopic analysis of the isomerization of 1-hexene at room temperature and at –40 °C reveal both markedly different binding behavior and product distribution, which provides support for the hypothesis that relative binding affinities of various alkene isomers have a strong influence on product selectivity.

In the ¹H NMR spectrum of the isomerization of 1-hexene with **5** at room temperature (Figure 7), the chemical shifts of

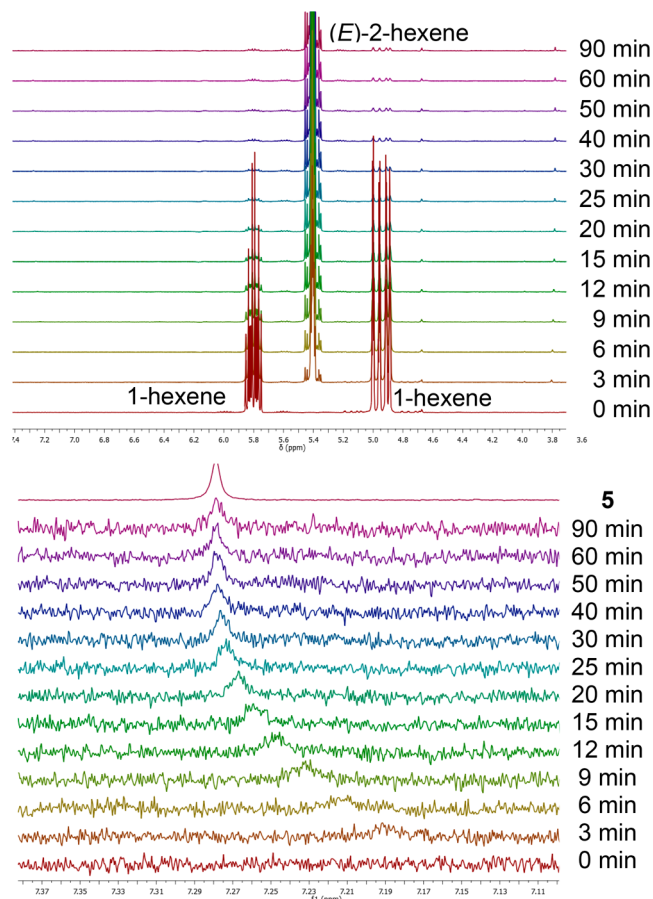


Figure 7. Stacked ¹H NMR spectra (500 MHz, acetone-*d*₆) of the first 90 min of isomerization of 1-hexene (0.5 M) with 0.3 mol % **5**. Top: Vinyl region indicating relative amounts of 1- and (*E*)-2-hexene. Bottom: Signal for C–H of imidazole.

protons associated with the catalyst monotonically change as the isomerization occurs. The changes suggest that the observed signal may arise from more than one species in fast equilibrium and that the concentrations of alkenes and their complexes are changing.

To slow alkene exchange and observe discrete alkene signals, data were acquired at –40 °C. The isomerization progress and catalyst monitoring are seen in Figure 8. Several significant

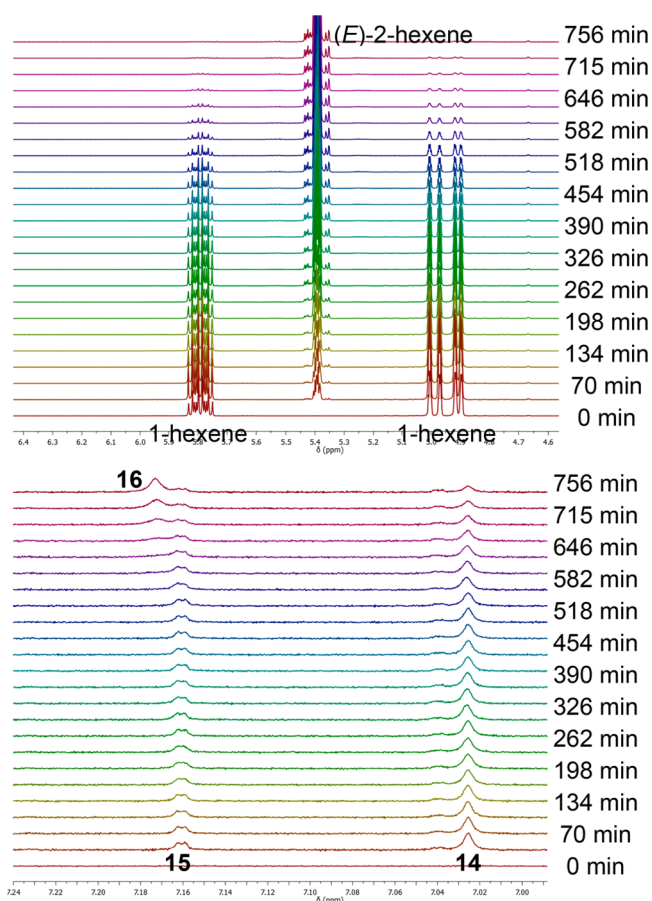


Figure 8. Isomerization of 1-hexene (0.5 M) at $-40\text{ }^{\circ}\text{C}$ (500 MHz, acetone- d_6) using 1.2 mol % **5**. Starting with the 0 min time point, the labels at right are for every other time point. Top: Vinyl region indicating relative amounts of 1- and (*E*)-2-hexene. Bottom: Signal for C5–H of imidazole of catalyst-derived species.

differences are apparent, most notably the decoalescence of the single signal for the imidazole C5–H. Initially, two major signals are present at 7.04 and 7.18 ppm in roughly a 2:1 ratio (Figure 8). While free catalyst **5** could be responsible for one of the two signals, the intensity of the signals does not vary much before 500 min, at which time both begin to decrease as a signal at 7.19 ppm emerges. Because alkene binding in the equilibrium $\text{5} + \text{alkene} \rightleftharpoons \text{5(alkene)}$ should be more favorable entropically at lower temperatures, we instead assigned the 7.04 and 7.18 ppm signals to two different diastereomers of **5**(1-hexene) (**14** and **15**, Chart 3), and the emerging 7.19 ppm signal to **5**(*E*)-2-hexene) (**16**, Chart 3).^{68a,b}

Then, we analyzed the room temperature data using what is observable at $-40\text{ }^{\circ}\text{C}$. In the lower part of Figure 7, the uppermost trace shows the C5–H signal for pure **5**. Observable 3 min after addition of 1-hexene, at which time 55% of the 1-hexene remains, is a broad signal with an upfield shift of 0.089 ppm relative to the signal for free **5** (Figure 9). The C5–H signal continues to migrate downfield as the reaction progresses with the $\Delta\delta$ (the difference in chemical shift from that of free catalyst **5**) becoming smaller until the reaction time approaches 40 min, after which $\Delta\delta$ does not change. Notably, the measured value for the chemical shift for the imidazole signal at the 40 min point (7.277 ppm) is only 0.002 ppm less than the signal for **5** in the absence of alkene and hence experimentally identical. We hypothesize that in

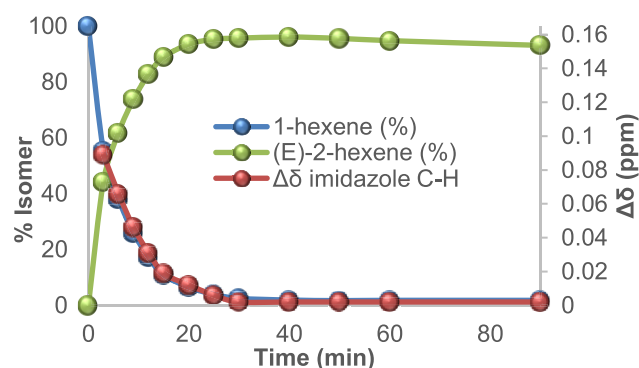
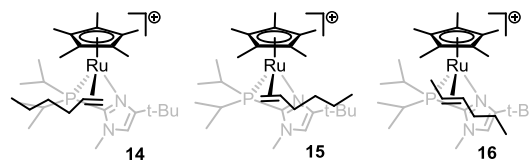


Figure 9. First 90 min of isomerization of 1-hexene (0.5 M) with 0.3 mol % **5** at room temperature. Graph of conversion of 1-hexene into (*E*)-2-hexene and the $\Delta\delta$ of C5–H signal of the imidazole ring on the PN ligand, where $\Delta\delta$ is the difference in chemical shift from that of free catalyst **5** (see text).

analogy to reaction at $-40\text{ }^{\circ}\text{C}$, there are two alkene complexes early in the reaction as well as free catalyst **5**. The two alkene complexes are bound **5**(1-hexene) complex (**14** and **15**, Chart 4) because the data suggest that formation of **5**(*E*)-2-hexene)

Chart 4. Putative Observed Alkene Complexes in Low-Temperature ($-40\text{ }^{\circ}\text{C}$) Isomerization of 1-Hexene



complex (**16**, Chart 4) is not nearly as favorable: the value of $\Delta\delta$ is largest when a large excess of 1-hexene is present early in the reaction and small and even zero when a large excess of (*E*)-2-hexene is present.

At room temperature, the rate of decrease in $\Delta\delta$ mirrors the rate of conversion of 1-hexene (Figure 9), which suggests that the concentration of the complexes are linked to the concentration of 1-hexene. If the observed imidazole CH chemical shift is a weighted average of the individual chemical shifts of protons in **5**, **14**, and **15**,⁶⁹ the relative concentrations of **5** and the alkene components can be determined by comparing the chemical shifts of intact catalyst **5** and of **5**(1-alkene) ($\Delta\delta/\Delta\delta_{100\%}$). To establish the chemical shift value for 100% bound complex, we used the weighted average (7.09 ppm) of the chemical shifts for the two imidazole C–H signals of complexes **14** and **15**, as measured at $-40\text{ }^{\circ}\text{C}$.

At room temperature, at the first time point (3 min) when 55% of 1-hexene remains, $\Delta\delta$ is $\sim 47\%$ of its maximum, which suggests 47% complexation and 53% free **5** despite a ~ 150 -fold excess of 1-hexene at this time point. The ratio of [1-hexene]/[**14** + **15**] remains consistent at $\sim 350:1$ until $<10\%$ of 1-hexene is left. Considering the constancy of the ratio, we project that $\sim 90\%$ of the catalyst contains bound alkene initially (when 100% of original 1-hexene is present, S/C ratio would be 333) and $\sim 87\%$ when 96% 1-hexene remains for a calculated value of 14 for $K_{b(1\text{-hexene})} = ([\text{14} + \text{15}]/[\text{5}][1\text{-hexene}])$

When the maximum amount of (*E*)-2-hexene is reached (96%), $\Delta\delta$ is around 1% of the maximum value, which suggests that 99% of catalyst is free of alkene. If the assumption is that

all of the alkene complexes are of (*E*)-2-hexene (even though this is not likely due to much more favorable binding of 1-hexene), we can establish an upper limit to the equilibrium binding constant for (*E*)-2-hexene ($K_{b((E)-2\text{-hexene})} = ([16]/[5][[(E)-2\text{-hexene}]])$), which is calculated to be ~ 0.02 . Thus, the ratio of $K_{b(1\text{-hexene})}/K_{b((E)-2\text{-hexene})}$ is evaluated to be at least 700:1 by this chemical shift perturbation method.

Then, we turned to further analysis of the data acquired at -40°C . Figure 10 shows graphs of the conversion of 1-hexene

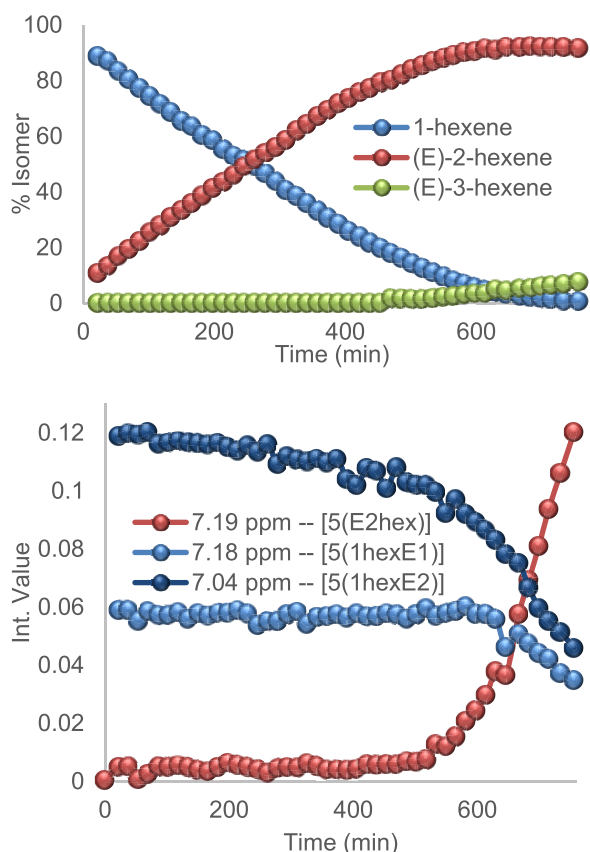


Figure 10. Isomerization of 1-hexene (0.5 M) at -40°C using 1.2 mol % **5** in acetone- d_6 . Top: Relative percentages of 1-hexene, (*E*)-2-hexene, and (*E*)-3-hexene over time. Bottom: Intensities of signals at 7.19, 7.18, and 7.04 ppm corresponding to imidazole C–H signal for 1- and (*E*)-2-hexene complexes.

at -40°C along with the relative intensities of the C–H imidazole signals for the three alkene complexes. The rate of conversion of 1-hexene at -40°C is unchanged over the first 500 min with a fit to linearity of $R^2 = 0.997$, which means that the rate is independent of the concentration of 1-alkene. The likely reason is that the catalyst is saturated with bound alkene throughout the first 500 min. Interestingly, the changes in the concentrations of the two 1-hexene complexes differ: the integration of the C–H signal at 7.18 ppm remains unchanged throughout the first 500 min, which would have to be constant if $d(1\text{-hexene})/dt = k[5]$. In contrast, the integration of the signal at 7.04 ppm decreases throughout the reaction. Because in only one of the diastereomers (**15**) does the allylic position appear to be in the right location to be deprotonated by the pendent imidazole, the other diastereomer **14** may not convert directly to product; we tentatively assign the 7.18 ppm signal to **15** and the 7.04 ppm signal to **14** where the latter may have to convert to the former through alkene decoordination–

coordination, but further work will be needed to evaluate our hypothesis. Finally, the signal at 7.19 ppm representing complex **16** (**5**((*E*)-2-hexene)) grows in when the amount of 1-hexene has dipped below 20% of its initial value.

A comparison of the relative stabilities of **14** + **15** and **16** (and therefore the relative binding affinities of 1-hexene and (*E*)-2-hexene) can be made by comparing the composition of the mixture of hexene isomers when the concentrations of bound 1-hexene and (*E*)-2-hexene are equal. At 715 min, the sum of the intensities of the signals at 7.04 and 7.18 ppm roughly equals the intensity of the signal at 7.19 ppm. At that point, the percentages of 1-hexene and (*E*)-2-hexene are 1.5 and 92.1%, respectively. We conclude that there is a 61-fold higher binding affinity for 1-hexene with **5** at -40°C . This ratio is lower than that calculated at room temperature ($\sim 700:1$) with the caveat that the two methods used to determine the ratios are not the same.

Systematic experimental comparisons of the binding of alkene isomers are rare, and such a study of binding to CpRuL_2^+ appears to be nonexistent; however, there are a fair number of studies with other metal fragments that compare a greater alkene steric and electronic diversity.⁷⁰ One approach is to determine binding equilibria $\text{L–M} + \text{alkene} \rightleftharpoons (\text{alkene})\text{M} + \text{L}$. Two-coordinate $\text{L–M} = (\text{nitrile})\text{Au}(\text{NHC})^+$ species do not seem to discriminate much in displacements.⁷¹ K_{eq} values follow: 1-hexene 25, propene 6.8, and *trans*- and *cis*-butene 12.5 and 38, respectively. Perhaps the closest study sterically to our case are five-coordinate species $(\text{nitrile})\text{Pd}(\text{PPh}_3)(\text{Cp})^+$.⁷² K_{eq} values follow: ethylene 13.5, propylene 1.14, and *trans*- and *cis*-2-butenes 0.04 and 0.22, respectively. Of particular note is the ratio of K_{eq} values for propylene and *trans*-2-butene: 28. Our hypothesis is that our six-coordinate complexes **5**(alkene) bearing rather bulky ligands are likely even more sensitive to alkene sterics. In support of this idea, we note Tolman's study of $\text{NiL}_3 + \text{alkene} \rightleftharpoons (\text{alkene})\text{NiL}_2 + \text{L}$, where $\text{L} = \text{P}(\text{O-ortho-tolyl})_3$.⁷³ K_{eq} values follow: 1-hexene, 0.5 and *trans*- and *cis*-2-hexenes, 0.0027 and 0.0022, respectively. Here, the selectivity for 1-hexene over (*E*)-2-hexene is 185:1.

To add insight as to why the binding affinity of (*E*)-2-hexene relative to that of 1-hexene should increase as temperature decreases, we computed the free energies and enthalpies of alkene and nitrile binding (Table 6). The difference in binding

Table 6. Computed Free Energies and Enthalpies of Binding with Catalyst/Alkene Complexes

catalyst	free energy (kcal/mol) ^a		enthalpy (kcal/mol) ^a	
	1-hexene	(<i>E</i>)-2-hexene	1-hexene	(<i>E</i>)-2-hexene
1 -CH ₃ CN ^b	11.4	10.4	17.0	16.0
5	6.1	4.1	14.1	13.5
6	2.7	0.3	10.7	8.7

^aGas phase calculation at 298 K. All values are relative to those for encounter complexes of alkene and catalyst. ^bWithout acetonitrile; Cp analogue of **5** that has yet to be detected or identified experimentally.

free energies of 1-hexene and (*E*)-2-hexene with **5** at room temperature (2.0 kcal/mol) is larger than the enthalpy difference (0.6 kcal/mol); therefore, as the entropic term decreases (i.e., at lower temperatures), the difference in binding affinity should decrease, as suggested from experiment. If positional selectivity is largely dictated by differences in binding affinities of terminal and internal alkenes, then isomerization should be less positionally selective at lower

temperatures provided the binding affinities are more similar, as suggested by computational and spectroscopic analysis. Evidence for this hypothesis is reflected in the lower selectivity for the formation of (*E*)-2-hexene at $-40\text{ }^{\circ}\text{C}$ with a maximum yield of (*E*)-2-hexene of 92% as opposed to 96% at room temperature. While other steps during the catalytic cycle can also play a factor in determining the relative rates of isomerization for the 1- to (*E*)-2-alkene and the (*E*)-2- to (*E*)-3-alkene, binding affinities clearly provide a strong contribution to the positional selectivity during catalysis with **5**, perhaps because **5** does not need to lose a ligand.

Alkene complex **5**(1-hexene) is computed to be 2 kcal/mol more stable than isomeric **5**((*E*)-2-hexene) for a ratio of 29:1 at 298 K. The 2 kcal/mol free energy difference is greater than the analogous difference for isomeric alkene complexes of catalyst **1** (1 kcal/mol) but less than for complexes of **6** (2.4 kcal/mol). The selectivity of the catalysts ($6 \approx 5 > 1$) mirrors the calculated preferences for 1-alkene binding ($6 \approx 5 > 1$).

Moreover, catalyst **1** had the largest computed binding affinities for both alkenes, while **6** exhibited the smallest. Substantiating the assumption that a favorable binding equilibrium leads to a higher rate of catalysis, the trend for binding affinities ($1 > 5 > 6$) also reflects the conversion rate, at least for the 1-alkene. The computational results show strong support for both the relative selectivities and relative rates of catalysts **1**, **5**, and **6**. Future work will explore individual mechanistic steps other than alkene binding using computations and kinetics.

Characterization of Allyl Intermediate. As shown in binding studies with ethylene, propylene, and 1-hexene, the coordinatively unsaturated nature of **5** provides for direct spectroscopic observation of alkene complexes. We aimed to find direct evidence for another key intermediate in the catalytic cycle that is consistent with the bifunctional mechanism proposed by ourselves^{38,41} and Fang⁷⁴ in which the phosphino-imidazole ligand acts as a pendant base, shuttling an allylic proton between carbons.

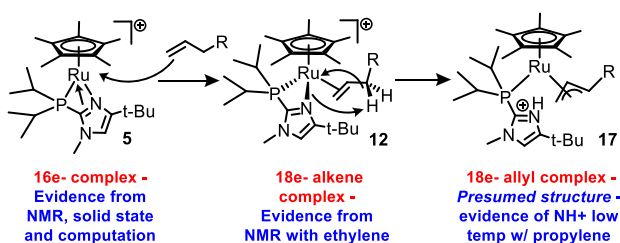
In addition to the major NMR signals that are assigned to **12** and **13** when introducing propylene to **5**, a number of small ^1H NMR signals corresponding to other minor species are present and are more noticeable at the reduced temperatures. Table S69 summarizes 1D and 2D ^1H , ^{13}C , and ^{15}N NMR data, from which we conclude that **12**, **13**, and **17** ($\text{R} = \text{H}$) can be formed in a ratio of approximately 4:1:1 (where the assignment of which signals belong to **12** and which to **13** is uncertain at this time). In the proposed intermediate (see structure **17**, $\text{R} = \text{H}$ in Scheme 3), the imidazole is protonated by the propylene, generating an allylic anion stabilized by the metal. One indication of **17** would be the presence of a downfield signal in the ^1H NMR spectrum corresponding to the N–H peak of the

protonated imidazole as well as downfield shift of the imidazole CH proton. At low temperatures (-30 to $-60\text{ }^{\circ}\text{C}$, Figures S75–S86), both a downfield shifted CH singlet at 7.75 ppm and a very downfield singlet assigned to the N–H proton are present at 12.4 ppm, which splits into a doublet ($J = 100\text{ Hz}$) when an ^{15}N -labeled ligand is used. The 12.4 ppm doublet is ascribed to the ^{15}N -H of an unchelated and protonated imidazole.⁷⁵ Further analysis of the mixture by 2D NMR leads to identification of most of the signals ascribable to **17** (Table S69 and Figure S96). However, because of the presence of multiple species (including the allyl, as one of the minor species) with overlapping peaks, assignment of the allyl protons and carbons remained tentative. Stronger direct evidence for allyl ligand signals was made possible by using $(^{13}\text{C})_3$ -propylene in 17:1 molar ratio with **5**. At $-40\text{ }^{\circ}\text{C}$, 3 sets of multiplets are visible in the ^{13}C NMR spectrum that can be ascribed to propylene-derived species: the first largest set at 134, 116, and 19 ppm from excess free propylene, the second set at 68, 60, 59, and 23 ppm ascribed to bound propylene complexes **12** and **13** (Scheme 2, and Figure 7), and a third, smaller set at 88 (t, $^1J_{\text{CC}} = 44.7\text{ Hz}$), 45 (d, $^1J_{\text{CC}} = 44.7\text{ Hz}$), and 41 (d, $^1J_{\text{CC}} = 44.7\text{ Hz}$) ppm⁷⁶ associated with the allyl species **17** (Figures S88–S94 and discussion in captions). The allyl complex and free propylene sets of signals are quite sharp, whereas the bound propylene signals are somewhat broad.

CONCLUSIONS

In summary, the coordinatively unsaturated Cp^*Ru catalyst **5** provides the same exceptionally high selectivity for (*E*)-2-alkenes as catalyst **2** + **2a** with yields usually exceeding 95% but with a dramatic increase in reaction efficiency (>400 times faster). Expedient isomerization occurs at room temperature with practical loadings of 0.1 to 0.5 mol % for most substrates, and commercial-grade substrates can be used after a simple deoxygenation. The binding and reactivity studies of **5** with alkenes, combined with computational modeling, depict the imidazole moiety on the diisopropyl(2-methyl-4-*tert*-butylimidazolyl)phosphine ligand as a hemilabile 4-electron donor. For the first time, we appreciate the full versatility of the pendent imidazole, which can change from 4-electron donation in **5**, where both the basic nitrogen lone pair and the imidazole π -system donate to the ruthenium, to 2-electron donation in 18-electron species such as alkene complexes derived from **5** and zero donation in allyl complex **17**, in which the imidazole is protonated, a range that is unique in $\text{Cp}^*\text{Ru}(\text{L})\text{X}$ chemistry where $\text{L} = \text{P}$ or N and $\text{X} = \text{P}$, N , or halide. In **5**, breaking the Ru–N bond of the $\kappa^2\text{-P,N}$ ligand provides two coordination sites for the allyl intermediate that is formed during catalysis, characterized here for the first time. UV–vis spectral data in conjunction with low- and room-temperature NMR data and kinetic analysis and computations have provided some initial insights into the role of alkene binding in achieving selectivity for monoisomerization. For the first time, we present direct experimental evidence in the form of **17** ($\text{R} = \text{H}$) for formation of an allyl complex from an alkene with protonation of the PN ligand. A more comprehensive mechanistic study of the isomerization mechanism, including not just alkene binding and allyl formation but alkene and allyl transformation steps on catalysts, is ongoing and will be reported in due course.

Scheme 3. Binding Modes of Imidazolyl Moiety and Alkene/Allyl Ligand



■ ASSOCIATED CONTENT

S Supporting Information

The Supporting Information is available free of charge on the ACS Publications website at DOI: 10.1021/acscatal.8b04345.

Synthetic and testing procedures, NMR and UV–vis spectral data, isomerization data, and computational data (PDF)

Crystallographic information for [Cp⁺RuCl]₄ (CIF)

Crystallographic information for 3 (CIF)

Crystallographic information for 5 (CIF)

Crystallographic information for 6 (CIF)

Crystallographic information for 7 (CIF)

Crystallographic information for 8 (CIF)

■ AUTHOR INFORMATION

Corresponding Author

*E-mail: dbgrotjahn@sdsu.edu.

ORCID

Curtis E. Moore: 0000-0002-3311-7155

David P. Pullman: 0000-0002-0437-5876

Douglas B. Grotjahn: 0000-0002-2481-7889

Notes

The authors declare the following competing financial interest(s): Catalyst 5 is covered by US Patent 9708236 (July 18, 2017) on which D.B.G. and E.R.P. are two of the inventors, but it is not currently sold commercially.

■ ACKNOWLEDGMENTS

We would like to thank Braden Silva for his advice and training for the computational chemistry and Drs. LeRoy Lafferty and Bennett Addison for their assistance as directors of the San Diego State University NMR facility. We also thank Thomas Chi Cao for first identifying alkene complexes in reaction mixtures using complex 1 (manuscript in preparation). Experimental work was supported by NSF Awards CHE-1059107, CHE-1464781, and CHE-1800598. Computational work is made possible by support from CHE-0947087.

■ REFERENCES

- (1) Bouziane, A.; Carboni, B.; Bruneau, C.; Carreaux, F.; Renaud, J.-L. Pentamethylcyclopentadienyl Ruthenium: an Efficient Catalyst for the Redox Isomerization of Functionalized Allylic Alcohols into Carbonyl Compounds. *Tetrahedron* **2008**, *64*, 11745.
- (2) Uma, R.; Crevisy, C.; Gree, R. Transposition of Allylic Alcohols into Carbonyl Compounds Mediated by Transition Metal Complexes. *Chem. Rev.* **2003**, *103*, 27.
- (3) Kuznik, N.; Krompiec, S. Transition Metal Complexes as Catalysts of Double-bond Migration in O-allyl Systems. *Coord. Chem. Rev.* **2007**, *251*, 222.
- (4) Krompiec, S.; Krompiec, M.; Penczek, R.; Ignasiak, H. Double bond Migration in N-allylic Systems Catalyzed by Transition Metal Complexes. *Coord. Chem. Rev.* **2008**, *252*, 1819.
- (5) For an overview of positionally selective isomerization catalysts, see ref 5 from our 2014 publication (ref 10).
- (6) Liu, X.; Zhang, W.; Wang, Y.; Zhang, Z.-X.; Jiao, L.; Liu, Q. Cobalt-Catalyzed Regioselective Olefin Isomerization Under Kinetic Control. *J. Am. Chem. Soc.* **2018**, *140*, 6873.
- (7) Chen, C.; Dugan, T. R.; Brennessel, W. W.; Weix, D. J.; Holland, P. L. Z-Selective Alkene Isomerization by High-Spin Cobalt(II) Complexes. *J. Am. Chem. Soc.* **2014**, *136*, 945–955.
- (8) (a) Schmidt, A.; Nodling, A. R.; Hilt, G. An Alternative Mechanism for the Cobalt-Catalyzed Isomerization of Terminal Alkenes to (Z)-2-Alkenes. *Angew. Chem., Int. Ed.* **2015**, *54*, 801.

(b) Weber, F.; Schmidt, A.; Rose, P.; Fischer, M.; Burghaus, O.; Hilt, G. Double-Bond Isomerization: Highly Reactive Nickel Catalyst Applied in the Synthesis of the Pheromone (9Z, 12Z)-Tetradeca-9–12-dienyl Acetate. *Org. Lett.* **2015**, *17*, 2952.

(9) Becica, J.; Glaze, O. D.; Wozniak, D. I.; Dobereiner, G. E. Selective Isomerization of Terminal Alkenes to (Z)-2-Alkenes Catalyzed by an Air-Stable Molybdenum(0) Complex. *Organometallics* **2018**, *37*, 482.

(10) Larsen, C. R.; Erdogan, G.; Grotjahn, D. B. General Catalyst Control of the Monoisomerization of 1-Alkenes to trans-2-Alkenes. *J. Am. Chem. Soc.* **2014**, *136*, 1226.

(11) Wang, Y.; Qin, C.; Jia, X.; Leng, X.; Huang, Z. An Agostic Iridium Pincer Complex as a Highly Efficient and Selective Catalyst for Monoisomerization of 1-Alkenes to trans-2-Alkenes. *Angew. Chem., Int. Ed.* **2017**, *56*, 1614.

(12) Hu, L.; Wu, Z.; Huang, G. Mechanism and Origins of Regio- and Stereoselectivities in Iridium-Catalyzed Isomerization of 1-Alkenes to trans-2-Alkenes. *Org. Lett.* **2018**, *20*, 5410.

(13) Grotjahn, D. B.; Larsen, C. R.; Erdogan, G. Bifunctional Catalyst Control of Alkene Isomerization. *Top. Catal.* **2014**, *57*, 1483.

(14) Campion, B. K.; Heyn, R. H.; Tilley, T. D. Preparation and Reactivity of 16-Electron 'Half-Sandwich' Ruthenium Complexes; X-Ray Crystal Structure of (η^5 -C₅Me₅)Ru(iPr₃P)Cl. *J. Chem. Soc., Chem. Commun.* **1988**, 278.

(15) Arluigie, T.; Border, C.; Chaudret, B.; Devillers, J.; Poilblanc, R. Chloro- and Hydrido(pentamethylcyclopentadienyl)ruthenium Complexes: Anomalous NMR Behavior of C₅Me₅RuH₃PR₃ (R = CHMe₂, Cy). *Organometallics* **1989**, *8*, 1308.

(16) Johnson, T. J.; Folting, K.; Streib, W. E.; Martin, J. D.; Huffman, J. C.; Jackson, S. A.; Eisenstein, O.; Caulton, K. G. π -Stabilized, yet Reactive, Half-Sandwich Cp^{*}Ru(PR₃)X Compounds: Synthesis, Structure, and Bonding. *Inorg. Chem.* **1995**, *34*, 488.

(17) Johnson, T. J.; Coan, P. S.; Caulton, K. C. Investigation of the Reactivity of Cp^{*}Ru(PiPr₂Ph)X toward H₂ and Silanes: Formation in Solution of Cp^{*}Ru(PiPr₂Ph)(H)₃ and Cp^{*}Ru(PiPr₂Ph)(H)₂Y (Y = Halide, OR, and SiR'₃). *Inorg. Chem.* **1993**, *32*, 4594.

(18) Streib, W. E.; Alota, A. A.; Caulton, K. G. Molecular Structure of Cp^{*}RuCl(PtBu₂Me). *Bull. Polym. Acad. Sci. Chem.* **1994**, *42*, 197.

(19) Jimenez-Tenorio, M.; Puerta, M. C.; Valerga, P. Synthesis and Properties of the 16-Electron Complex (C₅Me₅)RuCl(PMeiPr₂) and of Half-sandwich Ruthenium Hydrido Complexes Containing Bulky Monodentate Phosphine Ligands. *J. Organomet. Chem.* **2000**, *609*, 161.

(20) Rankin, M. A.; Hesp, K. D.; Schatte, G.; McDonald, R.; Stradiotto, M. Reactivity of a Coordinatively Unsaturated Cp^{*}Ru(κ^2 -P,O) Complex. *Chem. Commun.* **2008**, 250.

(21) Fasulo, M. E.; Glaser, P. B.; Tilley, T. D. Cp^{*}(PiPr₃)RuOTf: A Reagent for Access to Ruthenium Silylene Complexes. *Organometallics* **2011**, *30*, 5524.

(22) Gassman, P. G.; Mickelson, J. W.; Sowa, J. R. 1,2,3,4-Tetramethyl-5-(trifluoromethyl)cyclopentadienide: A Unique Ligand with the Steric Properties of Pentamethylcyclopentadienide and the Electronic Properties of Cyclopentadienide. *J. Am. Chem. Soc.* **1992**, *114*, 6942.

(23) Barthel-Rosa, L. P.; Sowa, J. R.; Gassman, P. G.; Fischer, J.; McCarty, B. M.; Goldsmith, S. L.; Gibson, M. T.; Nelson, J. H. Syntheses, Properties, and X-ray Crystal Structures of Iron and Ruthenium Compounds with the η^5 -C₅Me₄CF₃ Ligand. Compounds of the Type [(η^5 -C₅Me₄CF₃)M(μ -CO)(CO)₂] (M = Fe, Ru). *Organometallics* **1997**, *16*, 1595.

(24) Grotjahn, D. B. Bifunctional Catalysts and Related Complexes: Structures and Properties. *Dalton Trans.* **2008**, 6497, 6497.

(25) Rankin, M. A.; McDonald, R.; Ferguson, M. J.; Stradiotto, M. Exploring the Influence of Ancillary Ligand Charge and Geometry on the Properties of New Coordinatively Unsaturated Cp^{*}(κ^2 -P,N)Ru⁺ Complexes: Linkage Isomerism, Double C-H Bond Activation, and Reversible β -Hydride Elimination. *Organometallics* **2005**, *24*, 4981.

(26) Mauthner, K.; Slugovc, C.; Mereiter, K.; Schmid, R.; Kirchner, K. Synthesis and Reactivity of RuCp^{*}(κ^2 (P,N)-Ph₂PCH₂CH₂NMe₂)-

Cl. Chelate-Assisted Methyl C-H Activation and Formation of the Novel Complex $[\text{RuCp}^*(\kappa^3(\text{P},\text{N},\text{C})-\text{Ph}_2\text{PCH}_2\text{CH}_2\text{N}(\text{CH}_2)\text{Me})\text{Cl}]\text{-BPh}_4$. *Organometallics* **1997**, *16*, 1956.

(27) Ito, M.; Hirakawa, M.; Osaku, A.; Ikariya, T. Highly Efficient Chemoselective Hydrogenolysis of Epoxides Catalyzed by a $(\eta^5\text{-C}_5(\text{CH}_3)_5)\text{Ru}$ Complex Bearing a 2-(Diphenylphosphino)ethylamine Ligand. *Organometallics* **2003**, *22*, 4190.

(28) Ito, M.; Kitahara, S.; Ikariya, T. $\text{Cp}^*\text{Ru}(\text{PN})$ Complex-Catalyzed Isomerization of Allylic Alcohols and Its Application to the Asymmetric Synthesis of Muscone. *J. Am. Chem. Soc.* **2005**, *127*, 6172.

(29) Ito, M.; Osaku, A.; Shiibashi, A.; Ikariya, T. An Efficient Oxidative Lactonization of 1,4-Diols Catalyzed by $\text{Cp}^*\text{Ru}(\text{PN})$ Complexes. *Org. Lett.* **2007**, *9*, 1821.

(30) Across several different substrates, the reactions performed in situ with TIPF_6 show similar completion times: 2–4 h at 0.1 mol % and 15–30 min at 0.5 mol %, in some cases with excess TIPF_6 . In general, the in situ reactions were performed with TIPF_6 and the 1-alkene loaded into the J. Young tube, and an initial spectrum was taken; occasionally, the two compounds would be mixed several hours before the initial spectrum, and there was no evidence of isomerization prior to addition of complex 3.

(31) A variety of $\text{Ag}(\text{I})$ salts were tried and were decidedly inferior for reasons that are not entirely clear; see Table S1.

(32) Nagashima, H.; Kondo, H.; Hayashida, T.; Yamaguchi, Y.; Gondo, M.; Masuda, S.; Miyazaki, K.; Matsubara, K.; Kirchner, K. Chemistry of Coordinatively Unsaturated Organoruthenium Amidinates as Entry to Homogeneous Catalysis. *Coord. Chem. Rev.* **2003**, *245*, 177.

(33) Yamaguchi, Y.; Nagashima, H. $\text{C}_3\text{Me}_5\text{Ru}(\text{amidinate})$ Highly Reactive Ruthenium Complexes Formally Bearing 16 Valence Electrons Showing Signs of Coordinative Unsaturation. *Organometallics* **2000**, *19*, 725.

(34) Gemel, C.; Sapunov, V. N.; Mereiter, K.; Ferencic, M.; Schmid, R.; Kirchner, K. Cationic 16-Electron Half-sandwich Ruthenium Complexes Containing Asymmetric Diamines: Understanding the Stability and Reactivity of Coordinatively Unsaturated Two-legged Piano Stool Complexes. *Inorg. Chim. Acta* **1999**, *286*, 114.

(35) Phillips, A. D.; Thommes, K.; Scopelliti, R.; Gandolfi, C.; Albrecht, M.; Severin, K.; Schreiber, D. F.; Dyson, P. J. Modulating the Steric, Electronic, and Catalytic Properties of $\text{Cp}^*\text{Ruthenium}$ Half-Sandwich Complexes with β -Diketiminato Ligands. *Organometallics* **2011**, *30*, 6119.

(36) Palacios, M. D.; Puerta, M. C.; Valerga, P.; Lledos, A.; Veilly, E. Coordinatively Unsaturated Semisandwich Complexes of Ruthenium with Phosphinoamine Ligands and Related Species: A Complex Containing (R,R) -1,2-Bis((diisopropylphosphino)amino)cyclohexane in a New Coordination Form $\kappa^3\text{-P,P',N-}\eta^2\text{-PN}$. *Inorg. Chem.* **2007**, *46*, 6958.

(37) Rankin, M. A.; MacLean, D. F.; Schatte, G.; McDonald, R.; Stradiotto, M. Silylene Extrusion from Organosilanes via Double Geminal Si-H Bond Activation by a $\text{Cp}^*\text{Ru}(\kappa^2\text{-P,N})^+$ Complex: Observation of a Key Stoichiometric Step in the Glaser-Tilley Alkene Hydrosilylation Mechanism. *J. Am. Chem. Soc.* **2007**, *129*, 15855.

(38) Grotjahn, D. B.; Larsen, C. R.; Gustafson, J. L.; Nair, R.; Sharma, A. Extensive Isomerization of Alkenes Using a Bifunctional Catalyst: An Alkene Zipper. *J. Am. Chem. Soc.* **2007**, *129*, 9592.

(39) Ito, M.; Kitahara, S.; Ikariya, T. $\text{Cp}^*\text{Ru}(\text{PN})$ Complex-Catalyzed Isomerization of Allylic Alcohols and its Application to the Asymmetric Synthesis of Muscone. *J. Am. Chem. Soc.* **2005**, *127*, 6172.

(40) Larsen, C. R.; Grotjahn, D. B. Stereoselective Alkene Isomerization over One Position. *J. Am. Chem. Soc.* **2012**, *134*, 10357.

(41) Erdogan, G.; Grotjahn, D. B. Mild and Selective Deuteration and Isomerization of Alkenes by a Bifunctional Catalyst and Deuterium Oxide. *J. Am. Chem. Soc.* **2009**, *131*, 10354.

(42) Ito, M.; Sakaguchi, A.; Kobayashi, C.; Ikariya, T. Chemoselective Hydrogenation of Imides Catalyzed by $\text{Cp}^*\text{Ru}(\text{PN})$ Complexes and Its Application to the Asymmetric Synthesis of Paroxetine. *J. Am. Chem. Soc.* **2007**, *129*, 290.

(43) Ito, M.; Ootsuka, T.; Watari, R.; Shiibashi, A.; Himizu, A.; Ikariya, T. Catalytic Hydrogenation of Carboxamides and Esters by Well-Defined Cp^*Ru Complexes Bearing a Protic Amine Ligand. *J. Am. Chem. Soc.* **2011**, *133*, 4240.

(44) Lundgren, R. J.; Rankin, M. A.; McDonald, R.; Stradiotto, M. Neutral, Cationic, and Zwitterionic Ruthenium(II) Atom Transfer Radical Addition Catalysts Supported by P, N-Substituted Indene or Indenide Ligands. *Organometallics* **2008**, *27*, 254.

(45) Kelly, C. M.; Ruddy, A. J.; Wheaton, C. A.; Sydora, O. L.; Small, B. L.; Stradiotto, M.; Turculet, L. Synthesis, Structural Characterization, and Reactivity of $\text{Cp}^*\text{Ru}(\text{N-phosphinoamidinate})$ Complexes. *Can. J. Chem.* **2014**, *92*, 194.

(46) Doering, W. v. E.; Bragole, R. The Carbon Analog of the Claisen Rearrangement of Phenyl Allyl Ether. Equilibration of Butenylbenzenes and o-Propenyltoluenes. *Tetrahedron* **1966**, *22*, 385.

(47) Carleton, P. S. Conjugative Interaction of Benzene Rings and Double Bonds (Ph.D. Thesis). *Diss. Abstr. Int. B* **1967**, *27*, 4265.

(48) Doering, W. v. E.; Benkhoff, J.; Carleton, P. S.; Pagnotta, M. Conjugative Interaction in Styrenes. *J. Am. Chem. Soc.* **1997**, *119*, 10947.

(49) Hine, J.; Linden, S.-M.; Wang, A.; Thiagarajan, V. Double-Bond-Stabilizing Abilities of Dimethylamino, Alkylsulfonyl, and Acetyl Substituents. *J. Org. Chem.* **1980**, *45*, 2821.

(50) Larsen, C. R. A Novel Bifunctional Catalyst for Alkene Isomerization: Development, Scope and Limitations, and Applications in Organic Transformations. Ph.D. Thesis, San Diego State University and University of California, San Diego, 2012.

(51) Paulson, E. R.; Delgado, E.; Cooksy, A. L.; Grotjahn, D. B. Catalyst versus Substrate Control of Forming (*E*)-2-Alkenes from 1-Alkenes using Bifunctional Ruthenium Catalysts. *Org. Process Res. Dev.* **2018**, *22*, 1672.

(52) Gassman, P. G.; Macomber, D. W.; Hershberger, J. W. Evaluation by ESCA of the Electronic Effect of Methyl Substitution on the Cyclopentadienyl Ligand. A Study of Titanocenes, Zirconocenes. *Organometallics* **1983**, *2*, 1470.

(53) Sowa, J. R.; Angelici, R. J. Calorimetric Determination of the Heats of Protonation of the Metal in (Methyl-Substituted Cyclopentadienyl)Iridium Complexes, $\text{Cp}^*\text{Ir}(1,5\text{-COD})$. *J. Am. Chem. Soc.* **1991**, *113*, 2537.

(54) Lenges, C. P.; Brookhart, M. Isomerization of Aldehydes Catalyzed by Rhodium (I) Olefin Complexes. *Angew. Chem., Int. Ed.* **1999**, *38*, 3533.

(55) Zhang, H.-J.; Demerseman, B.; Xi, Z.; Bruneau, C. Ruthenium Complexes Bearing Bulky Pentasubstituted Cyclopentadienyl Ligands and Evaluation of $[\text{Ru}(\eta^5\text{-C}_5\text{Me}_4\text{R})(\text{MeCN})_3][\text{PF}_6]$ Precatalysts in Nucleophilic Allylic Substitution Reactions. *Eur. J. Inorg. Chem.* **2008**, *2008*, 3212.

(56) Mercier, A.; Yeo, W. C.; Chou, J.; Chaudhuri, P. D.; Bernardinelli, G.; Kundig, E. P. Synthesis of Highly Enantiomerically Enriched Planar Chiral Ruthenium Complexes via Pd-Catalyzed Asymmetric Hydrogenolysis. *Chem. Commun.* **2009**, 5227.

(57) Mercier, A.; Urbaneja, X.; Yeo, W. C.; Chaudhuri, P. D.; Cumming, G. R.; House, D.; Bernardinelli, G.; Kundig, E. P. Asymmetric Catalytic Hydrogenolysis of Aryl Halide Bonds in Fused Arene Chromium and Ruthenium Complexes. *Chem. - Eur. J.* **2010**, *16*, 6285.

(58) Wodrich, M. D.; Ye, B.; Gonthier, J. F.; Corminboeuf, C.; Cramer, N. Ligand-Controlled Regiodivergent Pathways of Rhodium-(III)-Catalyzed Dihydroisoquinolone Synthesis: Experimental and Computational Studies of Different Cyclopentadienyl Ligands. *Chem. - Eur. J.* **2014**, *20*, 15409.

(59) Hyster, T. K.; Dalton, D. M.; Rovis, T. Ligand Design for Rh(III)-Catalyzed C–H Activation: an Unsymmetrical Cyclopentadienyl Group Enables a Regioselective Synthesis of Dihydroisoquinolones. *Chem. Sci.* **2015**, *6*, 254.

(60) Oakdale, J. S.; Sit, R. K.; Fokin, V. V. Ruthenium-Catalyzed Cycloadditions of 1-Haloalkynes with Nitrile Oxides and Organic Azides: Synthesis of 4-Haloisoxazoles and 5-Halotriazoles. *Chem. - Eur. J.* **2014**, *20*, 11101.

(61) Nataro, C.; Thomas, L. M.; Angelici, R. J. Cyclopentadienyl Ligand Effects on Enthalpies of Protonation of the Ru-Ru Bond in Cp₂Ru₂(CO)₄ Complexes. *Inorg. Chem.* **1997**, *36*, 6000.

(62) Evju, J. K.; Mann, K. R. A Facile Route to 1-Trifluoromethyl-2,3,4,5-tetramethylcyclopentadienyl Ruthenium Half- and Mixed-Sandwich Compounds. *Organometallics* **2002**, *21*, 993.

(63) Multiwfn was used to determine the orbital composition for the computed orbitals in question. <http://sobereva.com/multiwfn/> accessed 12 May 2019. See also Lu, T.; Chen, F. Multiwfn: A Multifunctional Wavefunction Analyzer. *J. Comput. Chem.* **2012**, *33*, 580.

(64) Jimenez-Tenorio, M.; Puerta, M. C.; Valerga, P. Structure and Reactivity of Coordinatively Unsaturated Half-Sandwich Iron, Ruthenium and Osmium Complexes. *Eur. J. Inorg. Chem.* **2004**, *2004*, 17–32.

(65) Safo, M. K.; Gupta, G. P.; Walker, F. A.; Scheidt, W. R. Models of the Cytochromes b. Control of Axial Ligand Orientation with a "Hindered" Porphyrin System. *J. Am. Chem. Soc.* **1991**, *113*, 5497–5510.

(66) Bagherzadeh, M.; Tahsini, L.; Latifi, R. Efficient Oxidation of Olefins and Sulfides Catalyzed by Manganese(III)-tridentate Schiff Base Complex using UHP as Oxidant. *Catal. Commun.* **2008**, *9*, 1600.

(67) The initial drop in absorbance is likely greater because the absorbance increases over time after the initial drop, and the first spectrum is not acquired until 4 min.

(68) (a) The 7.19 ppm signal may include contribution from **5** or an adduct of **5** and either acetone solvent or of trace water. We note that the blue color of pure catalyst in solvent fades at temperatures between –20 and –40 °C but returns at warmer temperatures, consistent with an equilibrium $5 + L \rightleftharpoons 5(L)$ (L = solvent or water) being entropically favored at lower temperatures. Further work would be needed to clarify. Nonetheless, here we can use the assignment of the 7.19 ppm signal exclusively to **5**((*E*)-2-hexene) to give an upper bound for the amount of this internal alkene complex. (b) Just as there can be two diastereomers of **5**(1-hexene), for which we have some experimental evidence, there can be two diastereomers of **5**((*E*)-2-hexene). The single diastereomer **16** is shown because it could reasonably arise from **15** through an allyl intermediate, but the second diastereomer (neither pictured nor numbered) may be present. At this time, we have not detected two diastereomers of **5**((*E*)-2-hexene), but further work may do so.

(69) Kang, S. O.; Lynch, V. M.; Day, V. W.; Anslyn, E. V. Enthalpy- vs Entropy-Driven Complexation of Homoallylic Alcohols by Rhodium(I) Complexes. *Organometallics* **2011**, *30*, 6233.

(70) Johnson, J. B.; Rovis, T. More than Bystanders: The Effect of Olefins on Transition-Metal-Catalyzed Cross-Coupling Reactions. *Angew. Chem., Int. Ed.* **2008**, *47*, 840.

(71) Brown, T. J.; Dickens, M. G.; Widenhofer, R. A. Syntheses, X-ray Crystal Structures, and Solution Behavior of Monomeric, Cationic, Two-Coordinate Gold(I) π -Alkene Complexes. *J. Am. Chem. Soc.* **2009**, *131*, 6350.

(72) Kurosawa, H.; Majima, T.; Asada, N. Synthesis, Structures, Stabilities, and Reactions of Cationic Olefin Complexes of Palladium(II) Containing the η^5 -Cyclopentadienyl Ligand. *J. Am. Chem. Soc.* **1980**, *102*, 6996.

(73) Tolman, C. A. Formation Complexes of (Olefin)bis(tri-*o*-tolyl phosphite)nickel Complexes. *J. Am. Chem. Soc.* **1974**, *96*, 2780.

(74) Tao, J.; Sun, F.; Fang, T. Mechanism of Alkene Isomerization by Bifunctional Ruthenium Catalyst: A Theoretical Study. *J. Organomet. Chem.* **2012**, *698*, 1.

(75) Alei, M.; Morgan, L. O.; Wageman, W. E.; Whaley, T. W. pH Dependence of ¹⁵N NMR Shifts and Coupling Constants in Aqueous Imidazole and 1-Methylimidazole. Comments on Estimation of Tautomeric Equilibrium Constants for Aqueous Histidine. *J. Am. Chem. Soc.* **1980**, *102*, 2881.

(76) (a) Inspection of structures suggests that in **17** ($R = H$), the PN ligand is rotated so that the two ends of an η^3 -CH₂CHCH₂ ligand would be magnetically inequivalent, and at low temperatures needed to resolve NMR signals, we hypothesize that rotation of the bulky

metal fragment is slowed. (b) Because of the default digital resolution of the spectrum, coupling constant values are likely ± 0.5 Hz.